METEOROLOGICAL OFFICE
126767
9 MAY 1978
LIBRARY

MET O 11 TECHNICAL NOTE NO.106

AN EXPERIMENTAL FORECAST USING A NON-HYDROSTATIC MESOSCALE MODEL

by

K M CARPENTER

Meteorological Office (Met O 11)
London Road
Bracknell
Berkshire
United Kingdom

N.B. This paper has not been published. Permission to quote from it must be obtained from the Assistant Director of the above Meteorological Branch.

April 1978

MET O 11 TECHNICAL NOTE No. 106

AN EXPERIMENTAL FORECAST USING A NON-HYDROSTATIC MESOSCALE MODEL

by

K M Carpenter

ABSTRACT

The non-hydrostatic mesoscale model formulated by Tapp and White (1976) has been extended to include the effects of orography and the variation of the large scale meteorological situation. Other changes to the model, particularly in the parameterisation of surface exchanges and boundary layer turbulence, are described and its application as a forecasting tool is illustrated by an extensive study of one situation.

INTRODUCTION

Tapp and White (1976) have described the basic formulation of a non-hydrostatic meso-scale model. The distinguishing features of their limited area numerical model are that it has an upper boundary that can be placed at any height, that the map factor and the variation of the Coriolis parameter with latitude are ignored and, clearly, that it is non-hydrostatic. The variation of the map factor and the Coriolis parameter with latitude place an upper limit of a few thousand kilometres on the horizontal length scale of weather systems that the model can describe, but there is no lower limit to this length scale other than our current understanding of small scale turbulence. The model is thus an extremely flexible tool for the study of small scale and meso-scale systems (1km to 10^3km) and it is currently being used to simulate systems over a wide range of scales. One important reason for developing such a model was to produce local weather forecasts for the British Isles, and the purpose of this paper is to describe the first experiment of this nature. The version of the model used in this study was dry.

The situation chosen for the first weather forecast test of the model was that of the 14th June 1973, a day that was recommended to us by J E Simpson because of the vigorous sea breeze activity. Simpson, Mansfield and Milford (1977) have described a case study of the inland penetration and structure of a sea breeze front originating from the south coast of England on this date. It was considered particularly appropriate to use such a situation for the first test of the model because the weather systems of interest (sea breezes) are locally generated and can be described realistically without including the effects of water and orography in the model. Figure 1 shows the synoptic situation over a 24 hour period covering the forecast, and Figure 2, which is taken from Simpson et al (Figure 14), shows the surface pressure field and sea breeze fronts deduced from observations for 1800 GMT and 2200 GMT.

The remainder of this paper is divided into five section. In Section 2 the basic formulation is briefly reviewed and the main changes from the description of Tapp and White are noted. The surface exchanges and the treatment of boundary layer turbulence are discussed in Section 3, and a forecast for 1800 GMT on 14 June 1973 is presented. For this first forecast the lateral and upper boundary conditions are determined in a way that implies a static synoptic scale situation, and the effects of orography are excluded. This forecast is modified if orographic effects are considered, and a second forecast that is produced if orography is included in the model is presented in Section 4.

Section 5 contains a discussion of the lateral and upper boundary conditions and the method used to vary the large scale synoptic situation. The determination of the boundary conditions is of interest because there is no enhanced damping zone near the boundaries, and there is little distinction between inflow and outflow at the boundary. The use of upstream differencing at the first interior point ensures that the fields close to the boundary are smooth, and that the advective terms propagate information outwards at outflow points and inwards at inflow points. There is no control over the mass field at the upper or lateral boundaries, a feature that appears to produce no problems in spite of the comments of Anthes and Warner (1977).

Section 6 contains a discussion of some aspects of the results obtained with the object of gaining some insight into the dynamics of sea breezes. The two areas that are of most interest are the south coast, because it has been studied in detail by Simpson et al, and the N E Coast, where a marked shear line develops along the coast.

2. BASIC FORMULATION

The basic formulation of the model has changed very little from the description by Tapp and White. However, the equations used must be presented here for completeness and the opportunity is taken to list the small number of changes that have been made.

Equations of Motion

Density is eliminated from the equations for a compressible, diabatic non-hydrostatic atmosphere by introducing the Exner function P

$$P = \left(p/p_r \right)^{\kappa} \qquad 2.1$$

where p is pressure

p_r is a constant reference pressure and

$\kappa = R/c_p$ with R being the gas constant and c_p the specific heat at constant pressure

and the potential temperature θ

$$\theta = T/P \qquad 2.2$$

where T is temperature. Writing

$$\theta = \theta_0 + \theta_1 \qquad 2.3$$

where θ_0 is constant in space and time and

$$P = P_0 + P_1 \qquad 2.4$$

where P_0 satisfies the hydrostatic relation

$$\frac{\partial P_0}{\partial z} = - \frac{g}{c_p \theta_0} \qquad 2.5$$

i.e. $$P_0 = 1 - \frac{g z}{c_p \theta_0}$$

we obtain the basic model equations

$$\frac{\partial u}{\partial t} + c_p \theta_0 \frac{\partial P_1}{\partial x} = - \underset{\sim}{v} . \underset{\sim}{\nabla} u + f v - c_p \theta_1 \frac{\partial P_1}{\partial x} + F_1 \qquad 2.6$$

$$\frac{\partial v}{\partial t} + c_p \theta_0 \frac{\partial P_1}{\partial y} = - \underset{\sim}{v} . \underset{\sim}{\nabla} v - f u - c_p \theta_1 \frac{\partial P_1}{\partial y} + F_2 \qquad 2.7$$

$$\frac{\partial w}{\partial t} + c_p \theta_0 \frac{\partial P_1}{\partial z} = - \underset{\sim}{v} . \underset{\sim}{\nabla} w + g \frac{\theta_1}{\theta_0} - c_p \theta_1 \frac{\partial P_1}{\partial z} + F_3 \qquad 2.8$$

$$c_p \theta_0 \frac{\partial P_1}{\partial t} - g w + c_0^2 \underset{\sim}{\nabla} . \underset{\sim}{v} \qquad 2.9$$

$$= - c_p \theta_0 \left[\underset{\sim}{v} . \underset{\sim}{\nabla} P_1 + (\gamma - 1) P_1 \underset{\sim}{\nabla} . \underset{\sim}{v} - \frac{(\gamma - 1) Q}{c_p (\theta_0 + \theta_1)} \right]$$

$$\frac{\partial \theta_1}{\partial t} = - \underset{\sim}{v} . \underset{\sim}{\nabla} \theta_1 + \frac{Q}{c_p (P_0 + P_1)} \qquad 2.10$$

where u, v, w are the components of the velocity

$\underset{\sim}{v}$ in the x, y and z directions.

F_1, F_2 and F_3 are frictional terms

c_0^2 is the square of the speed of sound $(= \gamma R \theta_0 P_0)$

and Q is the diabatic heating.

As in Tapp and White, the terms that mediate sound waves have been written on the l.h.s. By using an implicit finite difference approximation for these terms it is possible to use time steps of about 90 secs in most conditions, independent of the horizontal grid length. This is comparable with the time steps used for hydrostatic models with a grid length of 10km. In practice other considerations are likely to limit the time step more severely e.g. the treatment of vertical boundary layer diffusion in convectively unstable conditions, which is discussed below, and, in a completely different use of the model, the description of cloud microphysics. The reader is referred to Tapp and White for a full discussion of the treatment of sound waves.

Lower Boundary Conditions

Equations 6 to 10 are approximated by second order accurate finite differences on a staggered grid, which is illustrated in Figure 3. Tapp and White imposed the lower boundary condition

$$w = 0 \qquad 2.11$$

at the lowest model level. Carpenter (1976) has noted the important effects achieved by varying the form of the vertical advection close to the lower boundary. In the present work, the lower boundary condition (equation 11) is imposed at ground level. This is done using the approximation(written here for a regular grid)

$$w \frac{\partial \chi}{\partial z} = \overline{w \, \delta_z \chi}^{z} \qquad 2.12$$

(in the notation of Shuman (1962)) and making $w \delta_z \chi$ vanish at ground level, whereas Tapp and White used

$$w \frac{\partial \chi}{\partial z} = \overline{w}^{z} \delta_{zz} \chi \qquad 2.13$$

and made $\overline{w}^{z} \delta_{zz} \chi$ vanish at the lowest model level. Equation 13 (mutatis mutandis) is still used to approximate the horizontal advection terms (except, as described in Section 5, at the lateral boundaries).

Time Smoothing

Several early integrations with the model showed various forms of time level separation, the oscillation between one time step and the next that is often a result of using the second order accurate leap-frog approximation for the time derivative terms.

$$\frac{\partial \chi}{\partial t}(t) = \frac{\chi(t+\delta t) - \chi(t-\delta t)}{2 \delta t} \qquad 2.14$$

In order to avoid this separation, and also to damp the 4 time step sound waves observed by Tapp and White, a time filter has been introduced (Asselin (1972))

$$\chi^*(t+\delta t) = \chi(t-\delta t) + 2\delta t \frac{\partial \chi}{\partial t}$$

$$\chi(t) = \mu(\chi(t-\delta t) + \chi^*(t+\delta t)) + (1-2\mu)\chi^*(t) \qquad 2.15$$

The value used for μ is 0.02.

Convective Adjustment

The original proposals of Tapp and White did not include explicitly any convective adjustment procedure or any parameterisation of cumulus activity, other than enhanced boundary layer diffusion in unstable conditions. This affected the early results in two ways. In a few isolated situations differential advection produced lapse rate instability and grid point storms developed, some of which could be seen to affect the overall forecast. Strong surface heating over land also led to grid point convection, which in this case was organised in a regular two grid length pattern. This regular convection was controlled to some extent by the large vertical diffusion used to represent boundary layer turbulence, but the roughness in the vertical velocities shown by Tapp and White (their figure 6) is due in part to this cause. It is difficult to find examples where the behaviour of the forecast after smoothing for output purposes has been affected by this roughness. Both these problems are now avoided by using a scheme that adjusts unstable or near neutral lapse rates between adjacent layers according to equation 16.

$$\frac{\partial}{\partial t}\frac{\partial \theta}{\partial z} = -\frac{1}{t^*}\left(\frac{\partial \theta}{\partial z} - \beta\right) \quad \text{if } \frac{\partial \theta}{\partial z} < \beta$$
$$= 0 \quad \text{if } \frac{\partial \theta}{\partial z} > \beta \qquad 2.16$$

The constant t^* is fixed at 10^3 secs and β is 3×10^{-4}km. This value for β is an order of magnitude lower than typical atmospheric values for the potential temperature lapse rate, and the value for t^* was chosen so that the relaxation of the lapse rate $\frac{\partial \theta}{\partial z}$ towards stability would be more rapid than likely values for the growth of the lapse rate instability or the destabilisation of the lapse rate by differential advection. The use of a non-vanishing equilibrium lapse rate β allows a larger value ~~than is otherwise the case~~ to be used for the relaxation time t^*, and also models, in a rough way, the fact that some areas within a grid box will be unstable in near neutral conditions.

Numerical Stability of Vertical Diffusion

The friction terms F_1 and F_2 and the diabatic term Q in equations 6, 7 and 10 include the boundary layer turbulence terms

$$F_1 = \frac{\partial}{\partial z} K_M \frac{\partial u}{\partial z} \qquad 2.17$$

$$F_2 = \frac{\partial}{\partial z} K_M \frac{\partial v}{\partial z} \qquad 2.18$$

$$Q/c_p\rho = \frac{\partial}{\partial z} K_H \frac{\partial \theta}{\partial z} \qquad 2.19$$

where K_M and K_H are eddy diffusivities for momentum and heat. If a simple

forward time step is used to approximate these terms, the value of the forward time step $2\delta t$ is limited by the usual stability criterion

$$2\delta t \leq \frac{\delta z^2}{2K} \qquad 2.20$$

where K is the appropriate eddy diffusivity. In unstable conditions and with the vertical grid used in the sea breeze simulations reported here, equation 20 unduly restricts the time step that can be used. This problem can be circumvented in a number of ways, but the method actually used is to integrate the vertical diffusion through 8 explicit short forward time steps (each $\delta t/4$) neglecting all other terms in the equation of motion. This is extremely simple, and stable for

$$2\delta t \leq 4\,\delta z^2/K \qquad 2.21$$

which is adequate in practice.

Diffusion

There have been several changes in the treatment of lateral and upper boundaries and these will be discussed in Section 5. The enhanced diffusion zone round the boundaries has been removed, but the horizontal diffusion constant has been increased from 0.3 to 0.5, so that the diffusion coefficient is now given by

$$K = 0.5\,\delta x^2\left[\left(\frac{\partial v}{\partial x}+\frac{\partial u}{\partial y}\right)^2+\frac{1}{2}\left\{\left(\frac{\partial u}{\partial x}\right)^2+\left(\frac{\partial v}{\partial y}\right)^2\right\}\right]^{1/2} \qquad 2.22$$

following Leith (1969). Tapp and White proposed the use of a Shapiro filter (Shapiro (1971)), but this was found to be ineffective when used infrequently and was abandoned.

Initial Conditions

The method that is used for the specification of initial conditions was described in Tapp and White (1976). The mass field is interpolated from data obtained from a larger scale model, the horizontal velocities are given by solving the Ekman layer equations and the vertical velocity is given by solving Richardson's equation.

$$\frac{D}{Dt}\left(c_p\theta\frac{\partial P}{\partial z}+g\right)=0 \qquad 2.23$$

Equation 23 gives

$$\frac{\partial^2 w}{\partial z^2}-\frac{\gamma g}{c^2}\frac{\partial w}{\partial z}=\frac{(\gamma-1)g}{c^2}\nabla_H\cdot\underset{\sim}{v}-\nabla_H\cdot\frac{\partial \underset{\sim}{v}}{\partial z}-\frac{1}{(\gamma-1)P}\underset{\sim}{\nabla}_H P\cdot\frac{\partial \underset{\sim}{v}}{\partial z} \qquad 2.24$$

so w must be given at the lower boundary, where w = 0, and at the upper boundary where it is prescribed by the larger scale model. Two aspects of this initialisation have been observed and deserve mention here.

The use of the Ekman layer equations to determine the horizontal velocities is not likely to be satisfactory for a deep model, where the inertial terms can be expected to be important outside the boundary layer. This limitation does not appear to have affected the present study.

The second problem arose in early experiments with the initialisation strictly as described above, which showed surface pressure increases of the order of 100 mb during a 24 hour forecast. This extreme rise in pressure was easily traced to an imposed net inflow of air, which arose because the present boundary conditions involve specifying the normal velocity. Since the continuity equation is not used in the initialisation, there is no control over the initial net inflow into the model volume, and the initialisation determines the net inflow throughout the integration. As a temporary expedient, this problem was overcome by changing the specified synoptic vertical velocity at the upper boundary in a way that implies a reasonable net inflow. In the process of experimenting with this feature of the initialisation it became clear that a large increase or decrease in average pressure had very little effect on any other aspect of the forecast, so the fact that the model cannot give a reliable forecast of average pressure, or that the average change in pressure must be imposed, is not regarded too seriously.

It is clear that further development of an appropriate initialisation programme is necessary, but the proposals of Tapp and White are quite adequate for the present study.

3. THE SURFACE EXCHANGES AND BOUNDARY LAYER TURBULENCE

In this section the calculation of the surface layer and boundary layer fluxes of heat and momentum are described. These two layers are regarded as completely separate, the only consistency that is required between them being continuity of the fluxes at the top of the surface layer. The calculation of the surface radiation budget is included in the surface exchanges.

Surface Exchanges

Since the current version of the model is dry and detailed radiation calculations are excluded, the only requirement of the surface exchanges scheme is that it gives good results for the surface sensible heat flux. However, a full surface exchanges scheme has been designed for the model and gives good results in the present context, so that scheme has been used and will be

described here. Earlier attempts to specify the surface temperature over the land and thus simplify some of the calculations proved unsatisfactory. However, over the sea the surface temperature is taken from the UK Meteorological Office sea temperature analysis and is held constant in time.

The equations are based on energy balance at the surface and thus the energy made available to the atmosphere as latent or sensible heat must be supplied by the residue from the radiation budget or, in principle but not in practice, ground heat storage. The incident solar energy S is specified

$$S = 510 \cos\left(\frac{\pi t}{12}\right) + 290 \qquad \text{M.K.S.} \qquad 3.1$$

where t is time in hours from midday.

This specification takes account of season (the summer solstice) and latitude, and allows for atmospheric absorption and reflection from the surface (about 35% for the combined effect). Thermal cooling of the surface B_o is given by

$$B_o = \sigma T_o^4 \qquad \text{M.K.S.} \qquad 3.2$$

where T_o is surface temperature and

σ is Steffan's constant

and the downward flux of thermal radiation is

$$B_1 = a\sigma T_1^4 \qquad \text{M.K.S.} \qquad 3.3$$

where a = 0.683 and T_1 is the temperature of the lowest model level.

Equation 3 is based on Brunt's law and Angstrom's formula as given in the Forecaster's Reference Book published by the UK Met Office. The value of the constant a corresponds to extremely dry air ($T_d \approx 272$K), and this is unrealistic. A more reasonable value for a would be about 0.72, indicating that the present value gives a deficit in the thermal warming of about 15M.K.S. There is no indication that this has had a serious effect on the results presented here, although it could give a 3K error in the surface temperature in equilibrium radiation conditions.

The net radiation R is given by

$$R = S + B_1 - B_o \qquad 3.4$$

and the surface energy balance equation is

$$R = H + LE + G \qquad 3.5$$

where H is the surface sensible heat flux
E is the surface humidity flux
G is the flux of heat into the ground and
L is the latent heat of vapourisation.

The turbulent fluxes of heat, moisture and momentum at the surface are given by the familiar bulk aerodynamic formulae

$$H = \rho_a c_p C_H |u| (\theta_s - \theta_a) \qquad 3.6$$

$$E = \rho_a C_H |u| (q_s - q_a) \qquad 3.7$$

$$\underset{\sim}{\tau} = -\rho_a C_D |u| \underset{\sim}{u} \qquad 3.8$$

where ρ_a is the density of air

C_D and C_H are bulk transfer coefficients

q_s and q_a are specific humidities at the surface and at the lowest model level and

θ_s and θ_a are potential temperatures at the surface and the lowest model level.

The calculation of C_D and C_H will be described below. Although the model is dry, the atmospheric humidity q_a is put equal to a constant value

$$q_a = .01 \qquad 3.9$$

in order to close the calculation of the surface exchanges. Over a dry surface, the evaporation must be supplied by transpiration through the vegetation, and this is described by a resistance formula (Monteith (1964))

$$E = \rho_a \frac{q_{sat}(\theta_s) - q_s}{r} \qquad 3.10$$

where $q_{sat}(\theta_s)$ is the saturated mixing ratio at the surface, and r is the resistence to 'evapotranspiration' (measured in seconds per metre). Resistence equations such as equation 10 are often used in micrometeorology, but I am not aware of any other example of their application in forecasting models. This is surprising, because the use of equation 10 to eliminate the surface

humidity q_s is straightforward, and the resulting equation

$$E = \rho_a \frac{1}{1 + r C_H |u|} C_H |u| (q_{sat}(\theta_s) - q_a) \qquad 3.11$$

gives a direct and well founded insight into the relation between actual and potential evaporation. Over wet surfaces, and where dew is forming ($E<0$), the surface resistence is put equal to zero (i.e. $q_s = q_{sat}(\theta_s)$)
The values that have been used for r are

r = 0 if $E < 0$ and over wet surfaces.
r = $100 sm^{-1}$ if $S > 0$, $E > 0$ i.e. during the day
r = $300 sm^{-1}$ if $S = 0$, $E > 0$ i.e. during the night.

The distinction between day and night is a crude representation of the response of plant physiology to diurnal variation. The value of $100 sm^{-1}$ is thought to be typical of forests, but rather high for grass (well irrigated meadow would give a value for r about $30 sm^{-1}$). Thus it is probably a reasonable value for a U.K. summer, but regional variations and irrigation by recent rainfall have been ignored.

The bulk transfer coefficients are calculated using tables based on Monin-Obukhov similarity theory. From the surface layer equations

$$\frac{\partial \theta}{\partial z} = \frac{\theta_*}{kz} \phi_H (z/L) \qquad 3.12$$

$$\frac{\partial u}{\partial z} = \frac{u_*}{kz} \phi_M (z/L) \qquad 3.13$$

and the definitions of θ_* and u_*

$$|\tau| = \rho_a C_D u^2 = \rho u_*^2$$

$$H = \rho_a c_p C_H |u| (\theta_s - \theta_a) = \rho_a c_p \theta_* u_*$$

it is easy to derive by integration

$$C_H = \frac{k^2}{\int_{\zeta_0}^{\zeta} \phi_M(\zeta) \frac{d\zeta}{\zeta} \int_{\zeta_0}^{\zeta} \phi_H(\zeta) \frac{d\zeta}{\zeta}} \qquad 3.14$$

$$C_D = \frac{k^2}{\left[\int_{\zeta_0}^{\zeta} \phi_M(\zeta) \frac{d\zeta}{\zeta} \right]^2} \qquad 3.15$$

where

$$\zeta = z/L$$

$$\zeta_0 = z_0/L$$

z_0 is the roughness length.

L is the Monin-Obukhov length

$$L = \left| \frac{C_D^{3/2}}{k C_H R_i} \right| z \qquad 3.16$$

R_i is the bulk Richardson number for the surface layer

$$R_i = \frac{g z}{\theta_a u^2} (\theta_a - \theta_s) \qquad 3.17$$

(neglecting the effect of humidity on buoyancy)

k is von Karman's constant, put equal to 0.4

and the expressions that have been used for the similarity functions and ϕ_M are ϕ_H

$$\phi = (1 + 5\, z/L) \qquad z/L \leq 1$$

$$\phi = 6 \qquad z/L > 1 \qquad 3.18$$

in stable conditions (Webb (1970)) and

$$\phi_M = (1 + 15\, z/L)^{-0.275}$$

$$\phi_H = (1 + 15\, z/L)^{-0.55} \qquad 3.19$$

in unstable conditions. (Dyer and Hicks (1970)).

Since ζ and ζ_0 are functions of R_i and z/z_0 only, the tables express C_D and C_H as functions of R_i and z/z_0 only.

In very unstable conditions, free convection similarity theory suggests

$$C_H = f_u(z/z_0) \sqrt{R_i} \qquad 3.20$$

The form of the function $f_u(z/z_0)$ has been determined by requiring that for any z/z_0, there is a value of R_i at which the transition from equation 14 to equation 20 is continuous and smooth. Below this transition value of R_i, equations 14 and 15 are used, but above this value of R_i equation 20 is used for C_H, and C_D is not varied with R_i. C_D and C_H are illustrated in Fig 4.

Over the land the roughness length could be made a function of the land use or type, but a constant value of 10 cm is used everywhere. In any event, the value used is only roughly representative of the average over a large area and this makes it inconsistent to use anything other than a constant value over

the sea. Accordingly, the value of z_0 for sea points is always 0.1 cm.

The heat flux into the ground is calculated using a two level model that is intended to reproduce the properties of uniform homogeneous soil. The equations governing the diffusion of heat in such an ideal medium are

$$\frac{\partial \theta(z,t)}{\partial t} = K_s \frac{\partial^2 \theta(z,t)}{\partial z^2} \qquad 3.21$$

$$K_s \left.\frac{\partial \theta}{\partial z}\right|_{z=0} = \frac{G}{\rho_s C_s} \qquad 3.22$$

where z is now depth into the ground
ρ_s is soil density
C_s is soil specific heat capacity and
K_s is soil thermal diffusivity.

By replacing z by

$$z' = z/\sqrt{K_s}$$

all parameters except $\rho_s C_s \sqrt{K_s}$ can be eliminated from 21 and 22. The scheme used to calculate the ground heat flux G in the model is a representation of 21 and 22

$$G = \rho_s C_s \sqrt{K_s} \left(\frac{1}{h_1} \frac{\partial \theta_s}{\partial t} + F \right) \qquad 3.23$$

$$F = \frac{1}{h_2} \frac{\partial \theta_g}{\partial t} = \lambda (\theta_s - \theta_g) \qquad 3.24$$

where h_1 = 43.5 M.K.S.
h_2 = 212 M.K.S.

and λ = 8.54 x 10^{-3} M.K.S. have been chosen so that equations 23 and 24 reproduce the properties of 21 and 22 for variation with periods of a day or less, and

θ_g is a "soil temperature".

Many comparison calculations indicate that equations 23 and 24 reproduce the properties of equations 21 and 22 very closely. However it should be remembered that even the idealised model equations 21 and 22 neglect the insulating effect of overlying vegetation, and the effect of temporal variations in the soil parameters ρ_s, C_s and K_s (e.g. due to rainfall and drainage).

The constant value used for $\rho_s C_s \sqrt{\lambda_s}$ is 950 M.K.S., which is a compromise between reasonable values for dry and moist soils. (Typical values for dry and for moist soils are 300 M.K.S and 1400 M.K.S. respectively). From equations 23 and 5 we can obtain a prognostic equation for θ_s ,

$$\frac{\partial \theta_s}{\partial t} = \frac{G}{\rho_s C_s \sqrt{\lambda_s}} - \lambda (\theta_s - \theta_g) \qquad 3.25$$

$$= \frac{R - H - LE}{\rho_s C_s \sqrt{\lambda_s}} - \lambda (\theta_s - \theta_g)$$

and this is the equation used to forecast surface temperature over the land.

The forecast heat fluxes for the clear summer day studied in this paper are shown, for a point in the Midlands (point A in Fig 11), in Fig 5. As stated above, the only requirement of the surface exchanges in the present context is that it gives reasonable values for the sensible heat flux, and it can be seen that this has been achieved.

Boundary Layer Turbulence

The effects of boundary layer turbulence are calculated using a K-theory flux/gradient approach. Thus the expression for the boundary layer turbulent diffusion of a general parameter χ is written

$$\left(\frac{\partial \chi}{\partial t}\right)_{turbulent} = \frac{\partial}{\partial z} K_\chi \frac{\partial}{\partial z} \chi \qquad 3.26$$

In principle, equation 26 is simply a definition of K_χ, but nearly all authors that use a K theory approach specify K_χ fairly arbitarily* (although in ways that are designed to reproduce observations) and the present work is no exception.

Close the surface, K_χ is chosen so that

$$K_\chi \frac{\partial \chi}{\partial z} = \overline{w' \chi'} \qquad 3.27$$

where $\overline{w'\chi'}$ (the vertical turbulent flux of χ at the surface) and the gradient of χ are determined using the surface layer equations 12 and 13.

Where the surface layer is unstable it is reasonable to suppose that a well mixed boundary layer with a well defined depth and a capping inversion will develop, and this situation has been well studied, e.g. Carson (1973),

*There is considerable interest e.g. Bodin (1976)Busch, Chang and Anthes (1976), Richards (1978) in the development of plausible arguments that provide a derivation of K_χ, but all such derivations include the specification of a vertical profile of the eddy mixing length, or some equivalent specification. Nevertheless most of these approaches are superior in some way to that presented in the text, which, except for its treatment of a capping inversion, is rather ad hoc.

Tennekes (1973). At the top of such a well mixed layer there is a downward flux of heat due to turbulent entrainment of air into the well mixed layer. This entrainment is driven predominantly by the surface heat flux, and it is found that the time development of the well mixed layer is well described if the downward heat flux is related directly to the upward surface heat flux. In the model context, these ideas are used by

(i) diagnosing from values held at the model levels the highest level within the mixed layer and thus the depth h_x of the well mixed layer

(ii) calculating $K_H^{(x)}$ at that level so that a downward heat flux is implied given by

$$K_H^{(x)} \frac{\partial \theta}{\partial z} = 0.2 \frac{H}{\rho c_p} \qquad 3.28$$

(Thus using equation 26 correctly, i.e. as a definition of the diffusion coefficient).

(iii) supposing that, at the level of the inversion, the mixing elements producing the downward flux of heat are forced and mix all other parameters in the same way i.e.

$$K_\chi^{(x)} = K_H^{(x)} \qquad 3.29$$

Thus, for an unstable surface layer, the depth of the layer with large values of K is known and, hopefully, reasonable values for K can be calculated at the top and at the bottom of the boundary layer.

For stable surface layers there is no deep thermally forced well mixed layer and it is reasonable to consider the boundary layer turbulence to be generated only by wind shear close to the surface. Earlier work with the present model used the profiles for K suggested by O'Brien (1970), and it seemed natural to continue with this approach in stable conditions. In order to ensure that there is no obviously unphysical discontinuity as the surface layer changes between stable and unstable, the ideas described above for the unstable case and the O'Brien profile for the stable case were included in a more general expression. The calculation of K at any height z is given by

$$K = 0.5 \qquad m^2/sec \qquad \text{for } z > h'$$

$$K = 0.5 + \left(\frac{h'-z}{h'-h_1}\right)^2 \left(1 + \left(\frac{h'+h_1}{h_1}\right)\left(\frac{z-h_1}{h'-h_1}\right)\right)(K_0 - 0.5) \quad \text{for } h' > z > h_x$$

$$K = 0.5 + \left(\frac{h'-z}{h'-h_1}\right)^2 \left(1 + \left(\frac{h'+h_1}{h_1}\right)\left(\frac{z-h_1}{h'-h_1}\right)\right)(K_0 - 0.5) \qquad 3.30$$

$$+ K_x \left(\frac{z-h_1}{h_x-h_1}\right)^2 \qquad m^2/sec \qquad \text{for } h_x > z > h_1$$

$$K = z/h_1 \; K_0 \qquad m^2/sec \qquad \text{for } h_1 > z$$

where $h' = h_2 \dfrac{h_2}{9h_x + 3h_2} + h_x = \dfrac{h_2}{3} + h_x \dfrac{3h_x}{3h_x + h_2}$ 3.31

$h_1 = .01 u_*/f$ in the height at which equation 27 is used

(ρu_*^2 is the surface stress)

K_x is the value of K for $z = h_x$

$h_2 = 25h_1 = .25 u_*/f$, which is intended as a calculation of the typical depth of the boundary layer given only the surface stress.

h_x is the depth of the mixed layer as described above

K_x is the value of K for $z = h_x$ given by equation 28.
(= 0 for a stable surface layer).

The estimate $h_2 = .25 u_*/f$ is based on observations of the neutral boundary layer and is likely to be an overestimate when the atmosphere is stably stratified in the surface and boundary layers. A stable (i.e. not neutral) boundary layer is indicated by $h_x = 0$, in which case equation 31 gives $h' = h_2/3$. For a neutral boundary layer $h_x \sim h_2$ and equation 31 gives $h' \sim h_2$ and where there is a deep, thermally driven mixed layer $h_x > h_2$ so that, from equation 31 $h_x < h' < \frac{13}{12} h_x$. The profile given for K by equation 30 is illustrated graphically in Figure 6.

Finally, a term is added to both diffusion coefficients K_M and K_H wherever a calculation of the local Richardson number R_i

$$R_i = \frac{g \; \partial\theta/\partial z}{\theta \left(\partial u/\partial z\right)^2} \qquad 3.32$$

indicates the presence of shear instability.

The term that is calculated is

$$f_u(R_i) \left|\frac{\partial u}{\partial z}\right| \delta z^2 \qquad 3.33$$

where $f_u(R_i) = 0.005$ for $R_i \leq 0$

$= 0.005 - 0.12 R_i^2 + 0.28 R_i^3$ for $0.25 \geq R_i \geq 0$

$= 0.00046875 / R_i$ for $R_i \geq 0.25$

has a maximum value of 0.005 for $R_i \leq 0$ and rapidly decreases for $R_i \geq 0.25$ and δz is the vertical separation of neighbouring model levels. This additional term is designed to remove a shear of 10 m/sec over a neutral layer 100 m thick in about 1 hour, and any function with the same general properties as $f_u(R_i)$ would be regarded as satisfactory.

Figure 7 shows the potential temperatures plotted against height forecast at two model points that are close to stations making routine radiosonde observations. It can be seen that the model describes quite well the development of a well mixed boundary layer, and the survival at night of an internal layer of low lapse rate, but that the overall temperature forecast is a few degrees too low. The coldness of the forecast could be due to the initial conditions, or to using too small a value for the subsidence over the whole of the U.K. in the prevailing anticyclonic conditions. A similar comparison between observations and the forecast wind profiles is not very satisfactory, and it appears that the present boundary layer turbulence parameterization, which is designed to describe the temperature structure of the thermally driven well mixed layer, is not likely to be appropriate for general application.

Forecast

The basic model with the surface exchanges and boundary layer schemes described above includes sufficient detail to make a forecast for the behaviour of sea breezes in static anticyclonic conditions. The U.K. Met. Office operational model, which produces forecasts on a 100km grid over the N.Atlantic and Europe, was used to provide a forecast of the synoptic situation at 0400 GMT on the 14 June 1973, and that forecast gave the initial conditions for an integration of the present small scale model. The effects of varying the synoptic situation (by allowing the high pressure cell to move towards the east) and the effects of orography were both excluded from this first integration, and these factors are discussed in later sections.

The forecast of surface pressure and winds at the lowest model level obtained for 1800 GMT on the 14th June 1973 are shown in Figure 8. A more detailed discussion of the quality of this forecast is postponed to Section 7, but a brief resume of the features that are of interest can be made immediately. Figure 2 shows the wind reports for the time of the forecast shown, and it also shows the position of the sea breeze fronts inferred by Simpson et al (1977).

With regard to the wind forecasts it is quite clear that they are veered from the observed winds, typically by about 45°. This discrepancy could be due either to the fact that the movement of the high pressure cell, which is held stationary in the forecast, implies a backing of the winds, or to the fact that the wind observations have been made close to the surface while the forecast is of winds at 50m.

The shear lines forecast in South and North Wales do not correspond to sea breeze fronts identified by Simpson et al, but there is little in the wind observations shown in Figure 2 to prove that these shear lines did not in fact occur. The sea breeze fronts shown in Figure 2 are both present in the forecast, but neither has penetrated far enough inland. It is natural to suppose that this is linked to the overall error in the forecast wind direction and evidence that this is the case, at least in part, will be presented later. The marked shear line forecast to lie along the NE coast was not noted by Simpson et al, but is very well supported by the observations.

4. OROGRAPHY

In order to include the effects of orography in the basic equations, equations 2.6 to 2.10, they were rewritten in terms of the vertical coordinate η

$$\eta = z - E(x,y) \qquad 4.1$$

where E is orographic height, and the perturbation P_1 of the Exner function P was redefined by

$$P = \left(p/p_r\right)^{R/c_p} = P_0 - \frac{gE}{c_p\theta_0} + P_1 \qquad 4.2$$

in place of equations 2.1 and 2.4. The vertical coordinate η and the resulting disposition of model levels is illustrated in Figure 9. Using equations 1 and 2 the basic equations become

$$\frac{Du}{Dt} = fv - c_p(\theta_0+\theta_1)\left(\frac{\partial P_1}{\partial x} - \frac{\partial E}{\partial x}\frac{\partial P_1}{\partial \eta}\right) = X \qquad 4.3$$

$$\frac{Dv}{Dt} = -fu - c_p(\theta_0+\theta_1)\left(\frac{\partial P_1}{\partial y} - \frac{\partial E}{\partial y}\frac{\partial P_1}{\partial \eta}\right) = Y \qquad 4.4$$

$$\frac{D\dot{\eta}}{Dt} = g\frac{\theta_1}{\theta_0} - c_p(\theta_0+\theta_1)\frac{\partial P_1}{\partial \eta} - \frac{\partial E}{\partial x}X - \frac{\partial E}{\partial y}Y - \left\{u^2\frac{\partial^2 E}{\partial x^2} + 2uv\frac{\partial^2 E}{\partial x \partial y} + v^2\frac{\partial^2 E}{\partial y^2}\right\} \qquad 4.5$$

$$\frac{DP_1}{Dt} = \frac{g}{c_p\theta_0}\left(\dot{\eta} + u\frac{\partial E}{\partial x} + v\frac{\partial E}{\partial y}\right) - (\gamma-1)\left(P_0 - \frac{gE}{c_p\theta_0} + P_1\right)\left(\frac{\partial u}{\partial x} + \frac{\partial v}{\partial y} + \frac{\partial \dot{\eta}}{\partial \eta}\right) + \frac{(\gamma-1)}{\theta_0+\theta_1}\left(P_0 - \frac{gE}{c_p\theta_0} + P_1\right)\frac{D\theta_1}{Dt} \qquad 4.6$$

$$\frac{D\theta_1}{Dt} = \frac{Q}{c_p P} \qquad 4.7$$

where frictional effects (i.e. the subgrid scale effects of the non-linear terms) have been excluded and

$$\frac{D}{Dt} = \frac{\partial}{\partial t} + u\frac{\partial}{\partial x} + v\frac{\partial}{\partial y} + \dot{\eta}\frac{\partial}{\partial \eta}$$

The vertical coordinate η and the expansion of the Exner function given by equation 2 were used because they lead to the simplest set of basic equations. In particular, the treatment of sound waves does not need to be modified if orography is included in this way. The implicit treatment of sound waves leads to Helmholtz equations of the form

$$\nabla_H^2 \Pi + \frac{\partial^2}{\partial \eta^2}\Pi - \frac{g}{c_p\theta_0}\frac{\partial}{\partial \eta}\Pi = \text{r.h.s.} \qquad 4.8$$

and it was found that any other vertical coordinate or expansion of P leads to terms that depend explicitly on position on the l.h.s. of this equation and thus reduce the range of techniques available for the solution of the Helmholtz equations.

The numerical solution of equations 3 to 7 and the basic decisions to use equations 1 and 2 are both being tested by making studies of air flow over isolated orography, and there is no sign in the studies to date that the use of a distorted coordinate system in the body of the fluid and at the upper boundary has any deleterious effect. Clark and Peltier (1977) and Clark (private communication) report that the grouping of the terms in equation 5 is important, and that equation 5 as it stands will lead to rough and non-conservative results. Experiments are being carried out into the effect of varying the finite difference approximation to the advective terms and writing equation 5 in the form

$$\frac{\partial \dot{\eta}}{\partial t} = - \underset{\sim}{u} \cdot \nabla \left(\dot{\eta} + u \frac{\partial E}{\partial x} + v \frac{\partial E}{\partial y} \right)$$
$$+ g \frac{\theta_1}{\theta_0} - c_p (\theta_0 + \theta_1) \frac{\partial P_1}{\partial \eta} \qquad 4.9$$
$$- \frac{\partial E}{\partial x} \left(X + \underset{\sim}{u} \cdot \nabla u \right) - \frac{\partial E}{\partial y} \left(Y + \underset{\sim}{u} \cdot \nabla v \right)$$

which should be more conservative and computationally more efficient.

At the upper boundary, the value of $\dot{\eta}$ is specified so that the flow is horizontal (or deviates from horizontal in accordance with the synoptic conditions)

$$\dot{\eta} = w_s - u \frac{\partial E}{\partial x} - v \frac{\partial E}{\partial y}$$

where w_s is an imposed real vertical velocity.

Further discussion of the nature of the upper boundary condition is postponed to Section 5, but it is noted here that, although no special measures are taken to ensure that gravity wave energy propagates out of the upper boundary (at 4km), there appears to be enough diffusion within the body of the fluid to ensure that gravity wave energy is propagated away from the surface. This is illustrated in Figure10, where the phase of the waves generated, in this case by sea breeze fronts, are seen to tilt up stream with height, except close to the upper boundary, implying the vertical propagation of wave energy.

Figure 11 shows the forecast given for 1800 GMT on 14th June 1973 when orography is included in the model, but no other changes are made from the model that gave the forecast shown in Figure 8. The orography itself is shown in Figure 12.

The overall forecasts and the behaviour of the sea breezes shown in Figures 8 and 11 are qualitatively very similar. The sea breezes are, in general, more advanced in the integration that includes orography, and this is probably due to an increase in the surface sensible heat flux, which is, in turn, a straightforward result of computing the surface exchanges at the orographic height above sea level. An increase in height results in a decrease in temperature and thus lower radiative cooling from the surface and a lower latent heat flux. There is also some channelling of the low level air flow e.g. up the Severn valley and possibly through the Midland Gap and round the Yorkshire Moors. The most striking difference between the forecasts is along the NE coast, where the inclusion of orography seems to have strengthened and deformed the shear line so that a cyclonic vortex is formed.

5. BOUNDARY CONDITIONS

Tapp and White (1976) described the method that was used to determine lateral and upper boundary values in early work with the present model. The treatment of the normal velocity and the pressure field at the boundary has not been changed, but the specification of potential temperature (given at inflow points and updated by advection only at outflow points) proved unsatisfactory in the present case study. The current procedure is summarised below.

(i) The normal velocity is imposed by interpolation of data from a larger scale model.

(ii) The pressure round the boundaries is determined from the normal pressure gradients calculated from the equations of motion perpendicular to the boundaries. This leads to Neumann (i.e. normal gradient) type boundary conditions for the Helmholtz equations describing the pressure field.

(iii) Tangential velocity and potential temperature at the boundary are both updated using the tendency observed at the previous time step at the first interior point. Specifically

$$\chi_0^{n+1} = \chi_0^{n} + \chi_1^{n} - \chi_1^{n-1} \qquad 5.1$$

where χ_0 is the boundary value of χ, which represents the field in question, χ_1 is the value of χ at the first interior point and the superscripts count the time increments.

(iv) Upstream differencing is used for the advection normal to the boundary at the first interior point.

(i) and (ii) imply rigid walls and a lid at the lateral and upper boundaries. It is clear that these conditions are not suitable for general applications of the model, and alternatives have been used in other applications, but they appear to be satisfactory in the present case study. It has already been pointed out (Figure 10) that gravity wave energy appears to propagate away from the surface, which is probably made possible by diffusion in the body of the fluid.

(iii) is best interpreted simply as a statement that the χ field is smooth close to the boundary. The use of the radiation-type boundary condition, equation 5.1, rather than a gradient condition e.g.

$$\chi_0^{n+1} = \chi_0^{*} + \chi_1^{n+1} - \chi_1^{*} \qquad 5.2$$

simplifies the coding and should reduce the reflection at the boundaries of waves in the χ field. Waves in the χ field with a group velocity $\delta x/\delta t$ will be wholly transmitted through the boundary.

The use of upstream advection (iv) at the first interior point is expedient because it leads to smoother fields and necessary because the use of centred advection in conjunction with equation 1 at inflow points is numerically unstable. It also has the theoretical advantage that it introduces a distinction between inflow points and outflow points, and it does this in a way that does not produce a sharp discontinuity when or where the flow switches from inflow to outflow. By using upstream advection in conjunction with equation 1, which in effect specifies the gradient of χ at the boundary, we ensure that the advective terms are calculated from imposed, large scale information at inflow points, but that no reference is made to imposed information about χ in the calculation of the advective terms at outflow points.

Experience to date indicates that (iii) and (iv) give smooth, convincing results. (Of course, this is not a proof that the results are correct !) On the other hand, the imposition of the normal velocity at the boundaries clearly leads to marked convergence and divergence at the boundaries and this feature of the present scheme requires further attention.

Varying the Synoptic Situation

Since the normal velocities at the boundaries are imposed, it is easy to vary their value according to a forecast by a larger scale model. In practice, this was carried out by creating initial data sets for the initial and final times, taking the difference and incrementing the normal velocities at the boundaries by an appropriate part of the difference at each time step. An experiment was carried out in which the normal velocities were corrected every hour, but this was unsatisfactory because the increments were too large and the time between boundary updates was very close to the time required for a horizontally propagating sound wave to transverse the grid twice. A resonant sound wave was excited on the scale of England ($\sim$ 600 km).

In view of (ii) above, no information about the varying pressure field was necessary in order to move the large scale features.

In order to increment the boundary values of tangential velocity and potential temperature in a way that is consistent with a changing synoptic situation, we observed that equation 1 can be rearranged

$$\chi_0^{n+1} - \chi_1^{n} = \text{constant} = -\delta x \frac{\partial \chi}{\partial n} + \delta t \frac{\partial \chi}{\partial t} \qquad 5.3$$

where $\frac{\partial \chi}{\partial n}$ is the space derivative of χ normal to the boundary. At any time, the value of the constant in equation 3 can be calculated from the present model fields or corrected in order to modify the large scale information. The initialised fields used to correct the normal velocities were also used to calculate current values of the constant in equation 2 (taking the average over 24 hours for $\frac{\partial \chi}{\partial t}$) at one hour intervals, and in the case of these fields this method proved satisfactory.

The initial surface pressure is shown in Figure 13. In figure 14 the final surface pressure interpolated from the large scale model is shown, and Figure 15 shows the final surface pressure forecast given by the present model. In this, admittedly slow moving, situation the present proposals for varying the synoptic situation have proved very successful.

The forecast of surface winds and sea level pressure at 1800 GMT without and with orography are shown in Figures 16 and 17. The expectation that the movement of the high pressure cell would improve the direction of surface wind forecasts is largely fulfilled, and the positions of all the sea breeze fronts are now closer to those observed by Simpson et al. As observed in the last section, the inclusion of orography increases the inland penetration of the sea breeze fronts, so that the south coast sea breeze is, if anything, too far inland when orography is included and the synoptic situation is varied.

6. DISCUSSION OF THE RESULTS

In this section we first show the forecast for several times that have been obtained, and then discuss two aspects of the forecast viz. the south coast sea breeze and the north-east coast shear line.

Results

The 50m wind forecasts for 1000 GMT, 1600 GMT, 2200 GMT and 0400 GMT are shown in Figure 18. The feature of this study that should be stressed is the potential that it shows for forecasting the high degree of local variability induced by orography and, particularly in this case, coastal topography. The vertical resolution of the boundary layer is very good by the comparison with most other large scale models and it should be possible to obtain all the advantages of high resolution one-dimensional models by making the best choice of heights for the levels. At the same time, the forecasts shown in Figure 18

make it clear that a one dimensional boundary layer model will not be adequate for making local weather forecasts on the basis of the large scale situation. The forecasts of 50m potential temperature shown in Figure 19 further illustrate this point. The thermal contrast at night between the surviving warm land air over the East Midlands and the relatively cold sea air over SE England is realistic and reasonable, and beyond the scope of any simpler model.

South Coast Sea Breeze

The work of Simpson et al(1977)emphasised the inland penetration of the south coast sea breeze on the 14th June 1973, and it is of interest to compare the present forecast with their observations. All four forecasts are shown in Figure 20. The inland penetration in the final forecast, which includes the effects of orography and the changing synoptic situation, is slightly excessive, probably because the surface sensible heat flux is too great in this version (see also Fig.7), but also confirming the earlier comments that the boundary layer turbulent transport of momentum are not very well modelled at present. The general behaviour of the inland penetration, in particular the evening acceleration of the sea breeze front, is in good agreement with the observations. Simpson et al attributed this acceleration to the increasing density contrast between the land and sea air, but two other mechanisms, present in reality and in the present model, also act to enhance this acceleration. The surface drag is greater during the day than at night, both because the surface drag coefficient is greater during the day, and because,in reality, the surface wind* is greater during the day due to the downward transport of momentum in the well mixed layer. The second mechanism is the cessation of the turbulent transfer of momentum across the upper boundary of the sea air. Simpson et al estimate that this mixing of land air moving offshore and sea air moving inland is of comparable importance to the surface exchanges of momentum.

Neumann (1977) has recently discussed the rotation of land and sea breezes. In the case of the south coast sea breeze it is interesting to note the long shore jet that develops in the latter part of the forecast period. This is illustrated in Figure 21, which shows a cross section of the westerly component of the wind at 22.00 GMT and also a cross section of potential temperature and the two dimensional wind vectors parallel to the section. This suggests that

*By and large the 50m winds forecast in the model increase at night because of the decoupling of the surface and the 50m level. The mechanisms producing the high wind speeds shown over S England in Fig 18 at 22Z and 04Z are probably similar to those producing the nocturnal jet often observed in anticyclonic situations over land.

sea breeze air moving inland rises at the sea breeze front and turns in the long shore direction as it does so, a movement that is illustrated by some of the particle trajectories in Figure 22.

North East Coast Shear Line

The aspect of the forecast that is least likely to be forecast reliably by a practical forecaster is the development of a marked shear line along the NE coast. The behaviour of this front again illustrates the results of Neumann (1977) since the onshore wind has shown a rapid veering into the long shore direction at the point where the synoptic offshore wind is greatest.

The inclusion of orography had a substantial effect on the behaviour of the sea breeze (see Figs 8 and 11). In order to clarify this point an experiment was carried out consisting of 3 forecasts, each for a restricted portion of the total forecast area. The 3 forecasts were

(i) no orography included, but the distinction between the land and the sea was retained

(ii) as (i), but with the part of the orography corresponding to the Yorkshire Moors retained (i.e. the main Pennine Chain was excluded, but the smaller approximately circular hill immediately adjacent to the coast was included - see Fig 12).

(iii) the distinction between land and sea was removed, but the Yorkshire Moors were included as in (ii).

Forecasts (i) and (ii) were very similar to each other and to the forecast shown in Figure 8, suggesting that the Yorkshire Moors had very little effect on the sea breeze and that the Pennines were the cause of the significant difference in the N.E. between Figs 8 and 11. Forecast (iii) showed some convergence over the hill due to the high level heating during the first two hours of the day, but the effect was negligible by comparison with the usual coastal sea breeze effect. This result can be compared with those reported by Mahrer and Pielke, (1977) but it should be noted that the Yorkshire Moors are a less pronounced feature than the coastal ridge that they considered and that the present offshore synoptic scale wind is stronger than any that they considered. Dalu (1978 and personal communication) has also noted the interaction between sea breezes and anabatic winds.

7. CONCLUSION

The forecast experiment reported in this paper is only the first of a series of experiments that must be carried out before the suitability for local weather forecasts of the non-hydrostatic meso-scale model described by Tapp and White (1976) can be assessed properly. In itself, the present work is encouraging both in its agreement with observations and in the nature and detail of the forecast. It must be concluded, from the results presented here, that a full three dimensional model is essential if local weather forecasts are to be obtained for the United Kingdom ~~on the basis of~~ from forecasts by synoptic scale models of the behaviour of the atmosphere on a larger scale.

REFERENCES

Anthes, R.A. and Warner, T.T. 1977 "The development of hydrostatic models suitable for air pollution and other meso-meteorological studies". Submitted to Mon.Weath.Rev.

Asselin, R. 1972 "Frequency filter for time integrations" Mon. Weath. Rev. 100, pp 487-490

Bodin, S 1976 "An unsteady one-dimensional atmospheric boundary layer model" WMO Symp. on the Int. of Broad Scale N.W.P. Prod. for local Forecasting, WMO No. 450 pp 20-26 (Ref 1.5)

Busch, N.E., Chang, S.W. and Anthes, R.A. 1976 "A multilevel model of the planetary boundary layer suitable for use with meso-scale dynamic models" J.Appl.Met. 15, pp 909-919

Carpenter, K.M. 1976 "Vertical advection at the lower boundary in a non-hydrostatic meso-scale model" Quart.J.R.Met Soc 102, pp 709-711

Carson, D.J. 1973 "The development of a dry inversion capped convectively unstable boundary layer" Quart. J.R. Met. Soc. 99, pp 450-467

Clark, T.L. and Peltier, W.R. 1977 "On the evolution and stability of finite amplitude mountain waves" J.Atmos Sci 34, pp 1715-1730

Dalu, G.A. "A parameterisation of heat convection for a numerical sea breeze model" Manuscript

Dyer A.J. and Hicks B.B. 1970 "Flux gradient relationships in the constant flux layer" Quart. J.R.Met.Soc. 96, pp 715-721

Leith, C.E. 1969 "Two dimensional eddy viscosity coefficients" Proc.WMO/IUGG Symp. on Num.Weath.Pred Japan Met Agency, Rep No. 67, pp 41-44

Mahrer,Y and Pielke R.A 1977 "The effects of topography on sea and land breezes in a two dimensional numerical model" Mon.Weath Rev. 105, pp 1151-1162

Monteith, J.L. 1964 "Evaporation and environment" Synop. Soc. Exp. Bio., 19 pp 205-234

Neumann, J. 1977 "On the rotation rate of the direction of sea and land breezes" J.Atmos. Sci. 34, pp 1913-1917

O'Brien, J.J 1970 "A note on the vertical structure of the eddy exchange coefficient in the planetary boundary layer" J.Atmos.Sci. 27, pp 1213-1215

Richards P.J.R.	1978	"The choice of eddy diffusion coefficients for a numerical model of the atmosphere" In preparation.
Schuman, F.G.	1962	"Numerical experiments with the primitive equations" Proc. Int. Symp. on Num.Weath.Pred., Japan Met. Agency; pp 85-106
Shapiro, R	1971	"The use of linear filtering as a parameterisation of atmospheric diffusion" J.Atmos. Sci. 28, pp 523-531
Simpson, J.E., Mansfield, D.A. and Milford J.R.	1977	"Inland penetration of sea-breeze fronts" Quart J.R.Met.Soc. 103, pp 47-76
Tapp, M.C. and White P.W.	1976	"A non-hydrostatic meso-scale model" Quart. J.R.Met.Soc. 102, pp 277-296
Tennekes, H.	1973	"A model for the dynamics of the inversion above a convective boundary layer" J.Atmos.Sci. 30 pp 558-567
Webb, E.K.	1970	"Profile relationships: the log-linear range, and extension to strong stability" Quart J.R.Met. Soc. 96, pp 67-90

FIGURE CAPTIONS

FIGURE 1. The synoptic situation over the U.K. on 14 June 1973.

FIGURE 2. Taken from Simpson et al (1977) (figure 14). Surface pressures and winds in England and Wales, 14 June 1973 (a) 1800 GMT, (b) 2200 GMT. The rows of circles show the position of sea breeze fronts.

FIGURE 3. (a) Staggering of the variables in the vertical. (b) Staggering of the variables in the horizontal.

FIGURE 4. The bulk transfer coefficients C_D (lower branch) and C_H (upper branch) for $R = \log z/z_o = 5,7,9$ and 11 as functions of the Richardson number (equation 3.17). The inset shows, for $\log z/z_o = 7$, the transition between the Dyer and Hicks (1970) formula (continued with a dotted line) and the free convection formula (continued with a dashed line).

FIGURE 5. The surface thermal energy balance calculated as described in the text for a point in the Midlands (Point A in Figure 12). The surface temperature is shown separately.

FIGURE 6. Illustration of the calculation of the boundary layer diffusion coefficient (equation 3.30) excluding the term due to shear (equation 3.33). The dotted line is the term included to obtain the correct downward heat flux through the inversion capping a well mixed layer; this term is added to the basic term (dashed line) to obtain the value used (solid line).

FIGURE 7. Forecast potential temperature at each model level for two grid points, one near Hemsby the other near Crawley. The observations at Hemsby and Crawley are shown by solid lines.

FIGURE 8. 50m winds and sea level pressure forecast for 1800 GMT on 14 June 1973 when orographic effects and the movement of the synoptic scale anticyclone are both neglected.

FIGURE 9. The vertical coordinate $\eta = z - E$, where z is the height above sea level and E in the orographic height. The model levels are parallel to the ground surface.

FIGURE 10. Cross sections of potential temperature and wind velocity parallel to the section (shown as arrows), forecast at 1800 GMT. The upper section is from B to C in Figure 12, the lower section is from points D to E in Figure 12.

FIGURE 11. 50m winds and sea level pressure forecast for 1800 GMT on 14 June 1973 when orography is included but the movement of the synoptic scale anticyclone is neglected.

FIGURE 12. U.K. orography used in the model. The locations named and point A are referred to in the text. Points B C D and E are referred to in other figures.

FIGURE 13. Initial sea level pressure (a) without orography (b) with orography.

FIGURE 14. Sea level pressure interpolated from a synoptic scale model (as for Figure 13) for the final time and used to derive the changes in the boundary conditions (a) without orography (b) with orography.

FIGURE 15. Forecast final sea level pressure. (a) without orography (b) with orography. This should be compared with figure 14.

FIGURE 16. 50m winds and sea level pressure forecast for 1800 GMT on 14 June 1973, neglecting the effects of orography but including the movement of the synoptic scale anticyclone.

FIGURE 17. 50m winds and sea level pressure forecast for 1800 GMT on 14 June 1973 when both orographic effects and the movement of the synoptic scale anticyclone are included.

FIGURE 18. 50m wind forecasts for 14 June 1973. Orography and synoptic scale changes were included in this forecast.

FIGURE 19. 50m potential temperature forecasts for 14 June 1973. Orography and synoptic scale changes were included in this forecast.

FIGURE 20. Inland penetration of the south coast sea breeze front. The observations are taken from Simpson et al (1977).

FIGURE 21. Cross sections from B to C (Figure 12) passing through the south coast sea breeze showing (a) the westerly component of the wind and (b) the potential temperature and wind velocity parallel to the section at 2200 GMT.

FIGURE 22. Calculated trajectories of fluid particles for the 24 hour forecast period. Particle heights are shown to the nearest 100m every 2 hours.

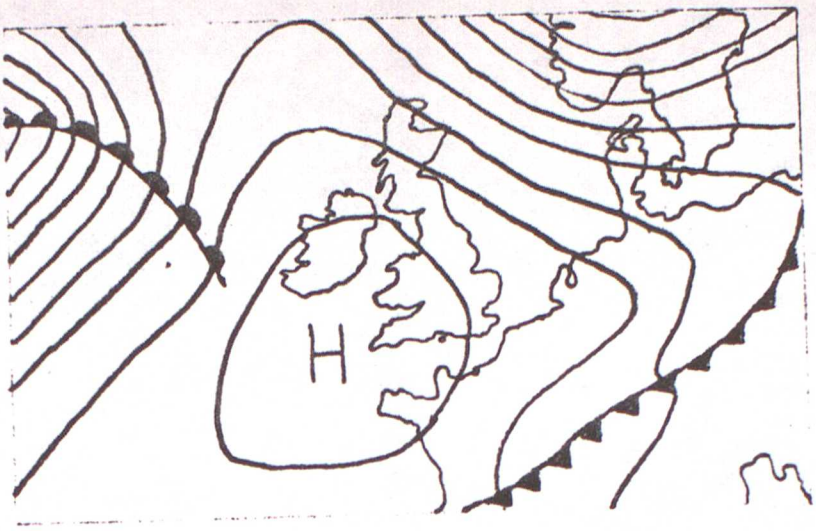

0000 G.M.T.

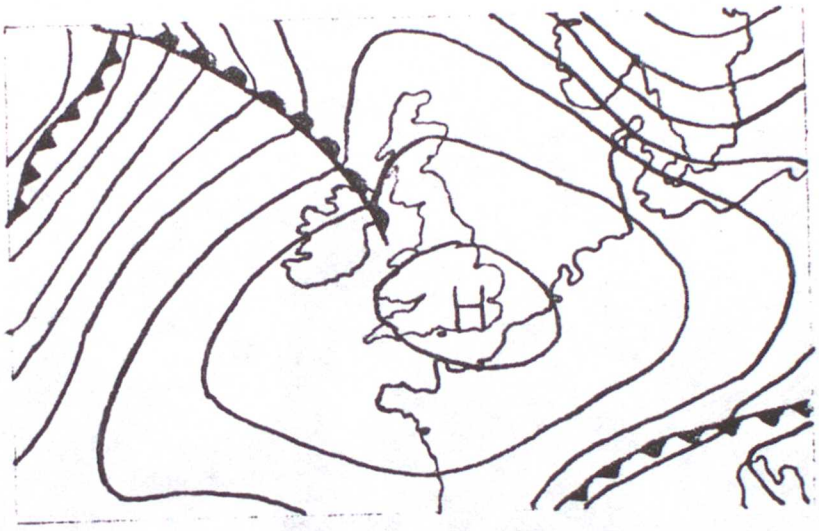

1200 G.M.T.

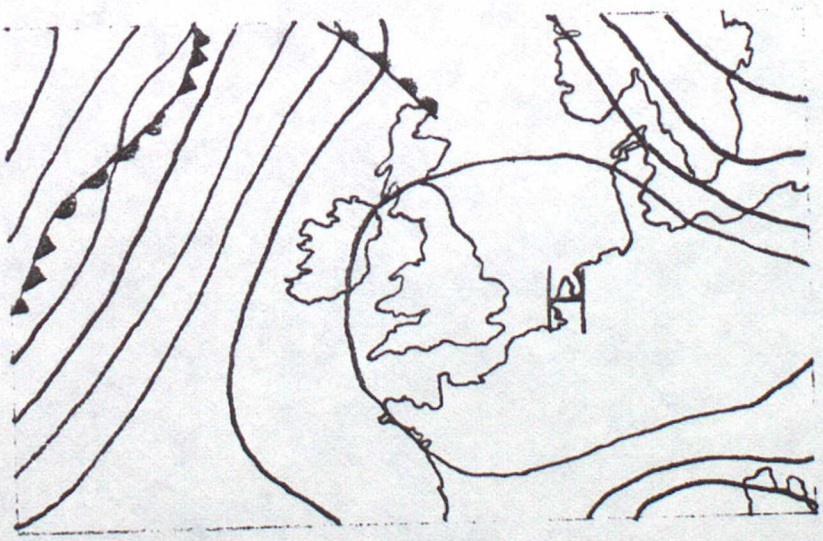

2400 G.M.T.

FIG 1

(a)

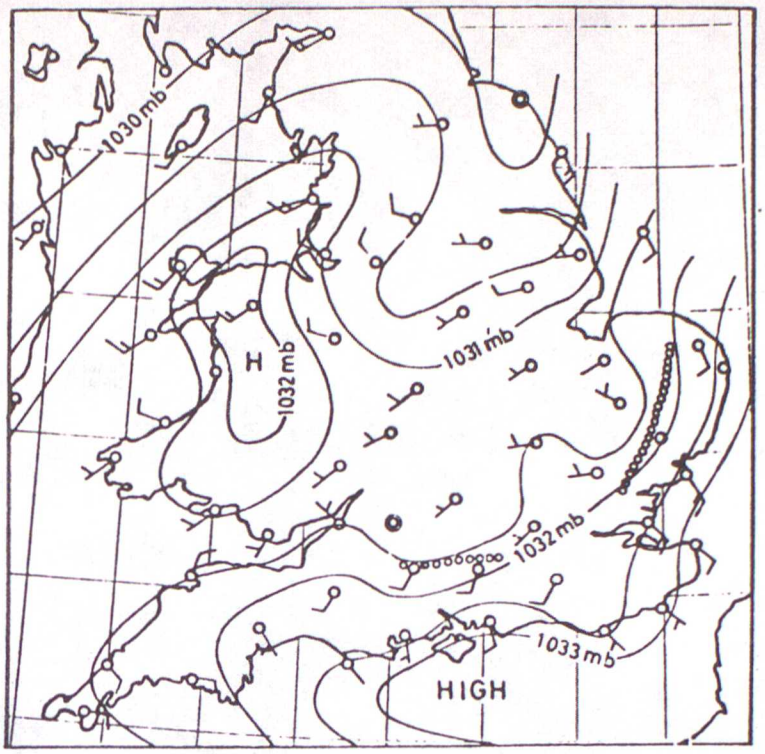

(b)

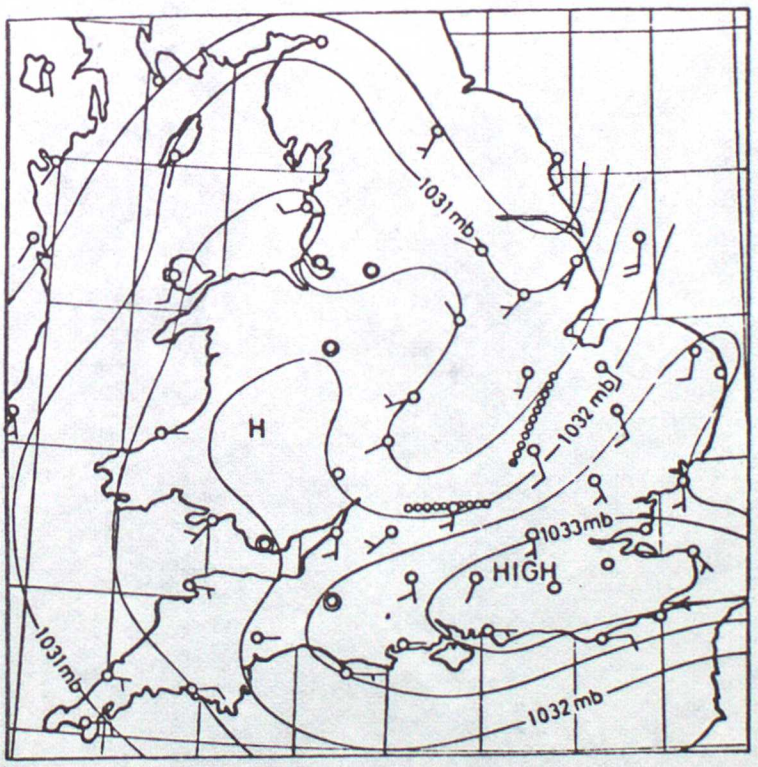

Figure 14. Surface pressure and winds in England, 14 June 1973. (a) 1800 GMT; (b) 2200 GMT. The rows of circles show the position of the sea-breeze fronts.

FIG 2

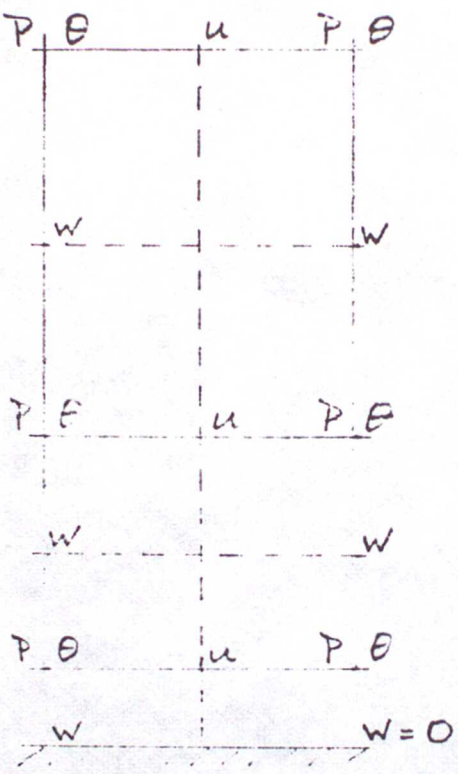

(a)

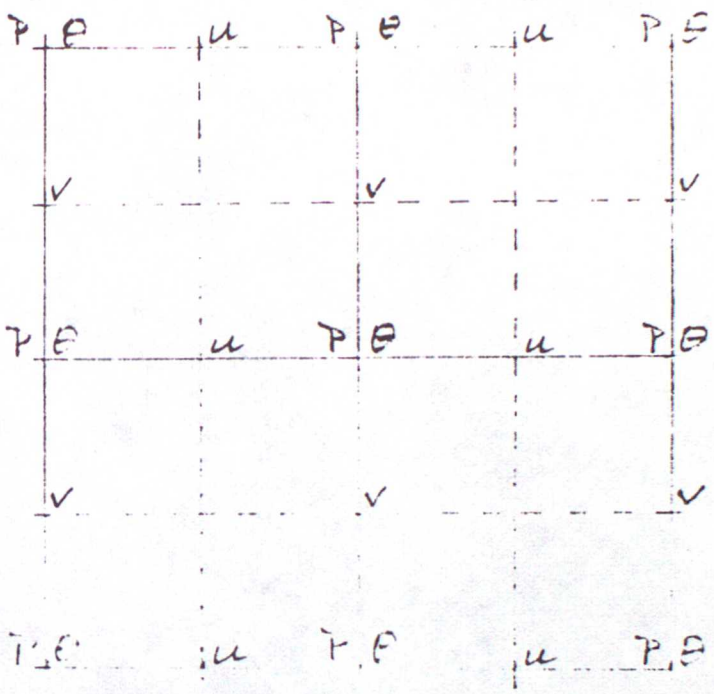

(b)

FIG 3

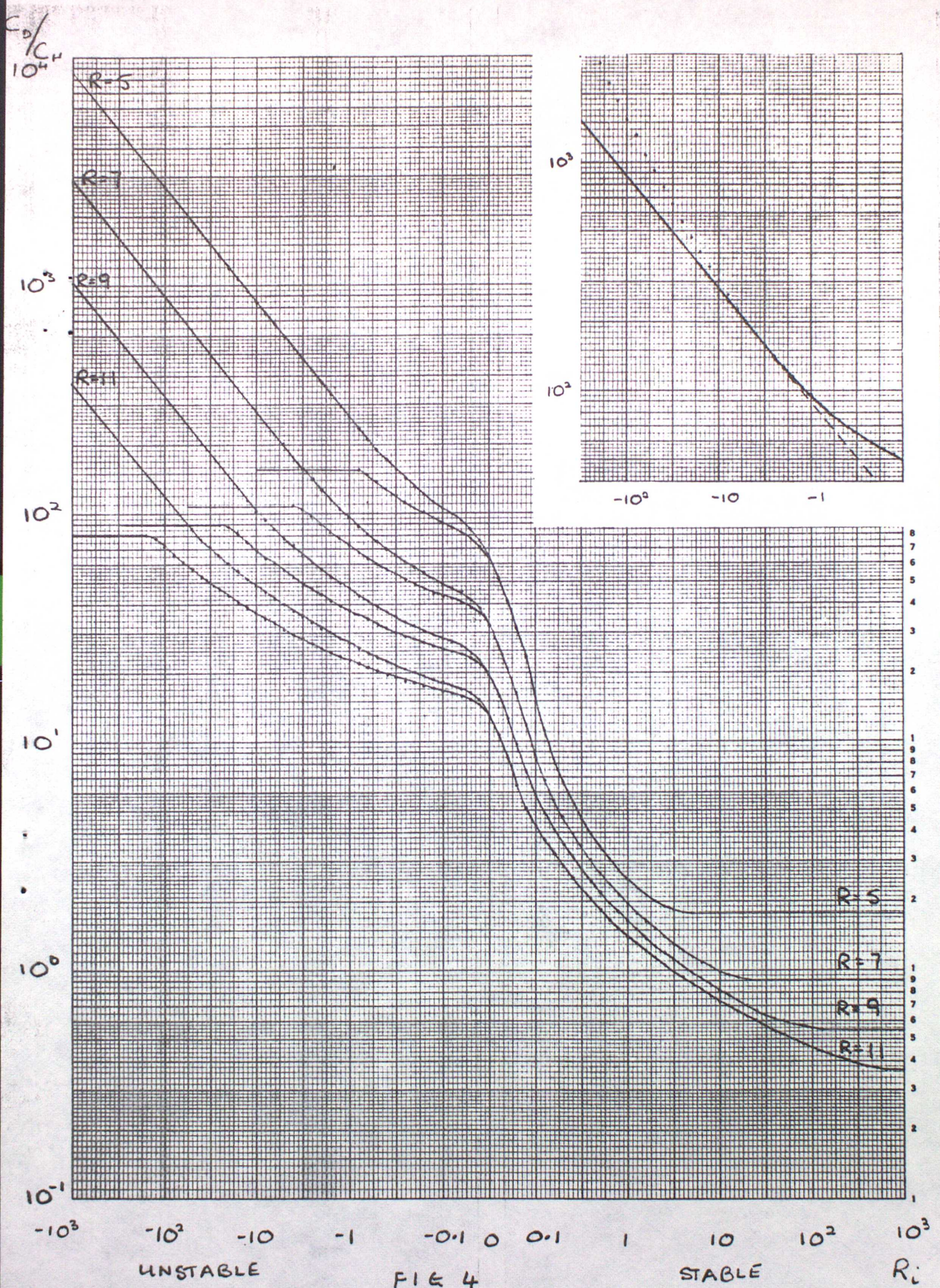
C_D/C_H
10^4
10^3
10^2
10^1
10^0
10^{-1}
R=5
R=7
R=9
R=11
10^3
10^2
-10^2
-10
-1
-10^3
-10^2
-10
-1
-0.1
0
0.1
1
10
10^2
10^3
UNSTABLE
STABLE
R_i

FIG 4

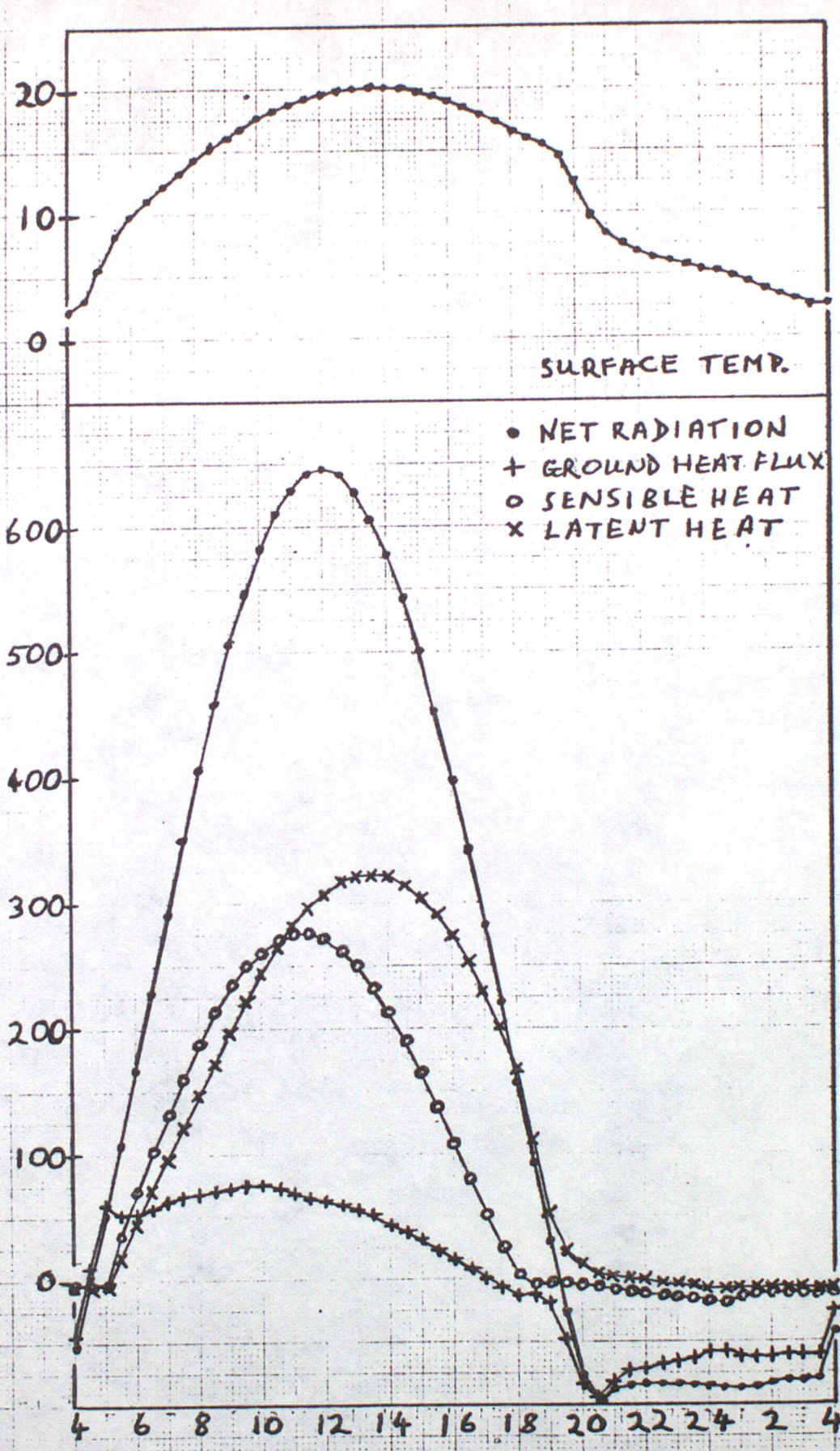
20
10
0
SURFACE TEMP.
• NET RADIATION
+ GROUND HEAT FLUX
o SENSIBLE HEAT
× LATENT HEAT
600
500
400
300
200
100
0
4 6 8 10 12 14 16 18 20 22 24 2 4

FIG 5

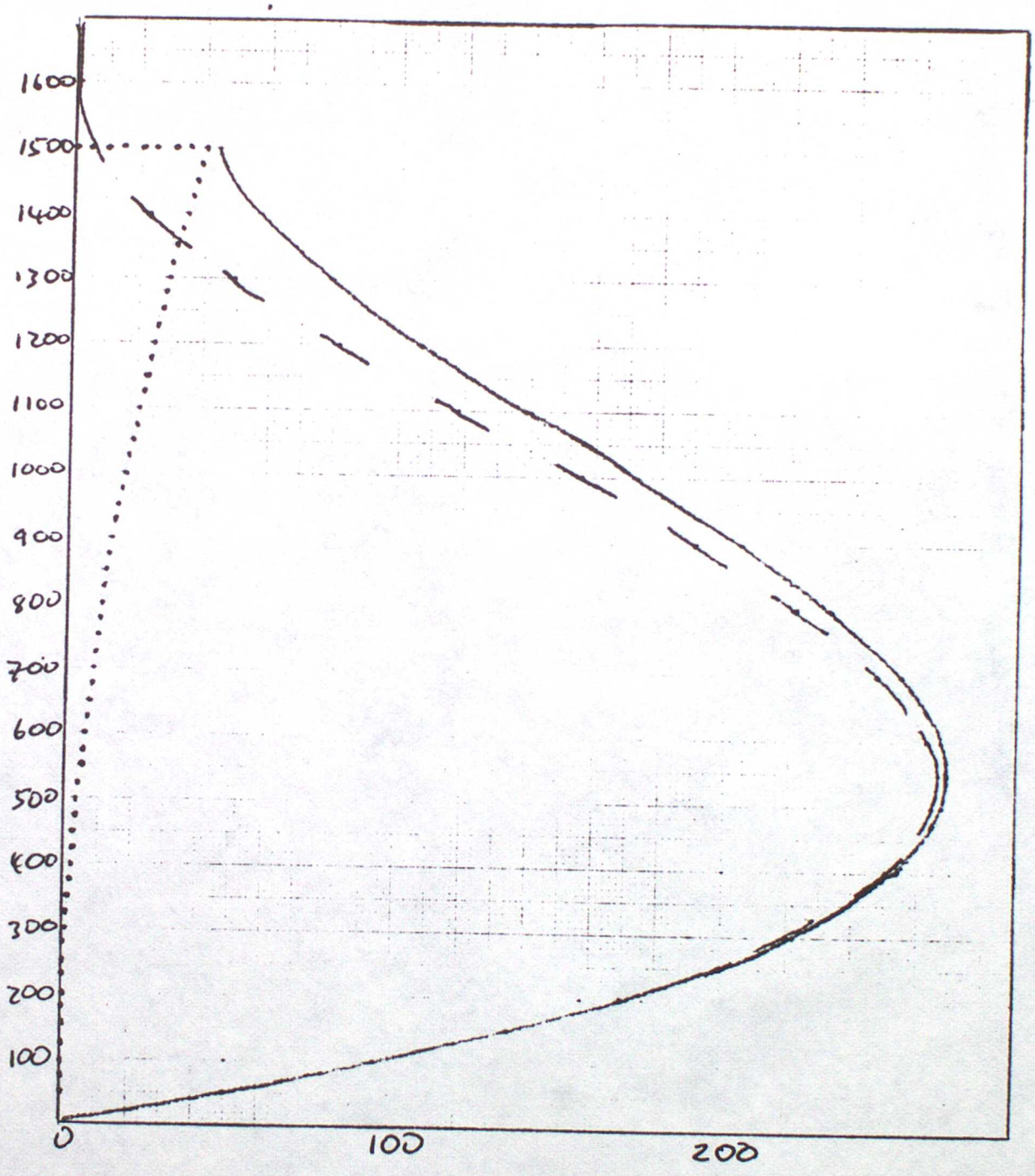
1600
1500
1400
1300
1200
1100
1000
900
800
700
600
500
400
300
200
100
0
100
200

FIG 6

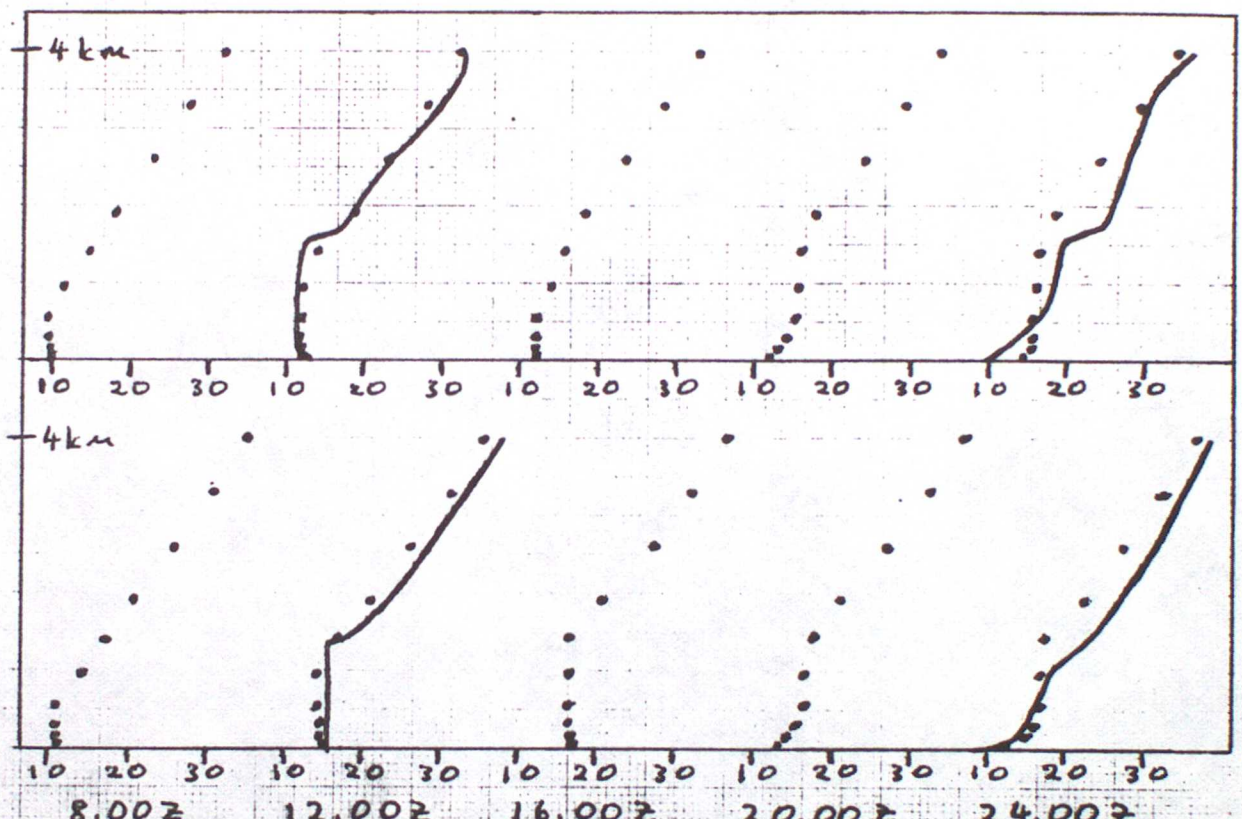

POTENTIAL TEMPERATURE • FORECAST
— OBSERVED

AT HEMSBY (TOP)
CRAWLEY (BOTTOM)

FIG. 7

1800 GMT

14 HR F'CAST MSL PRESSURE & LOW LEVEL WINDS

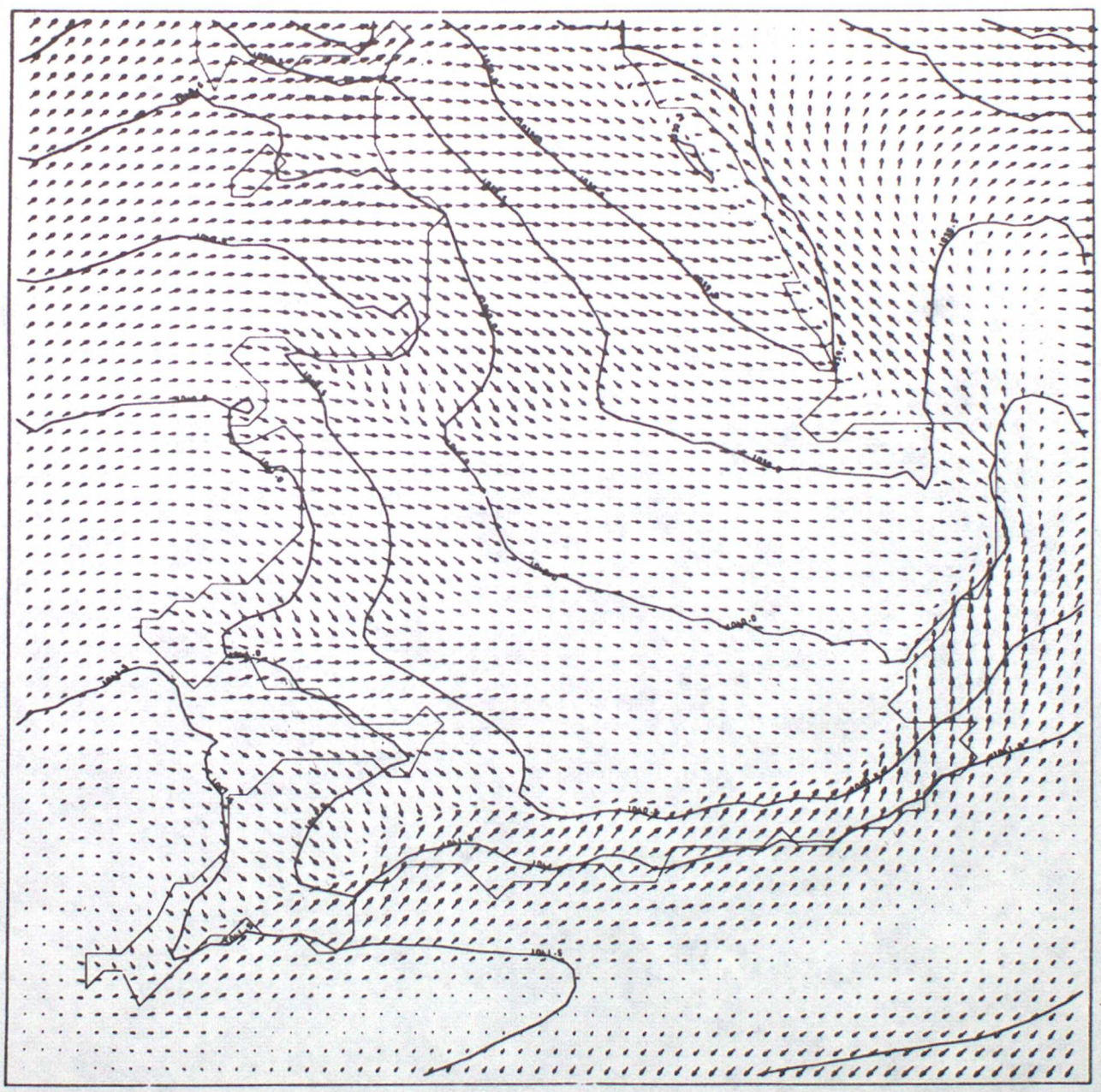

FIG. 8

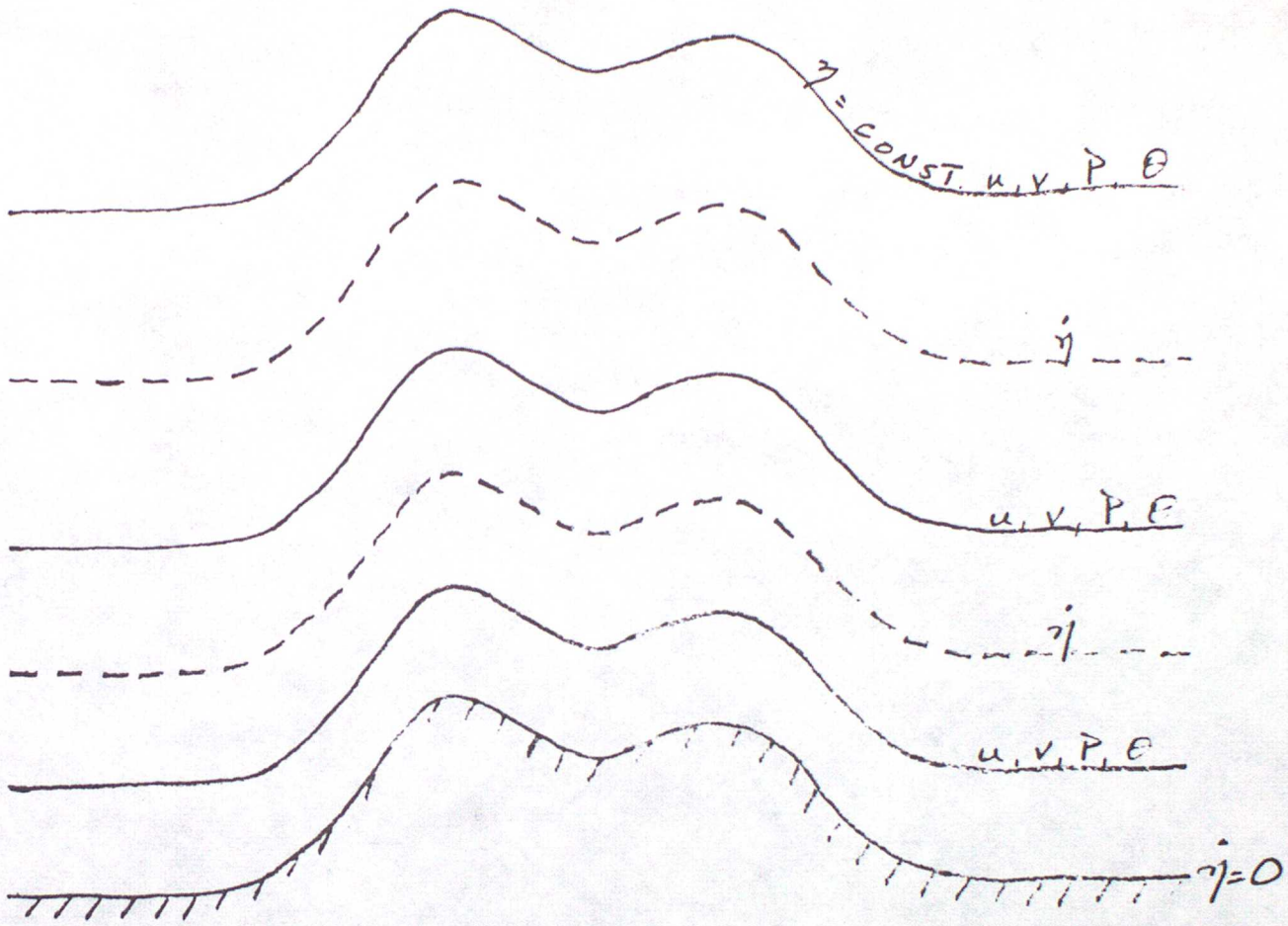

FIG. 9

1800 GMT

WIND VECTORS & POTENTIAL TEMPERATURE

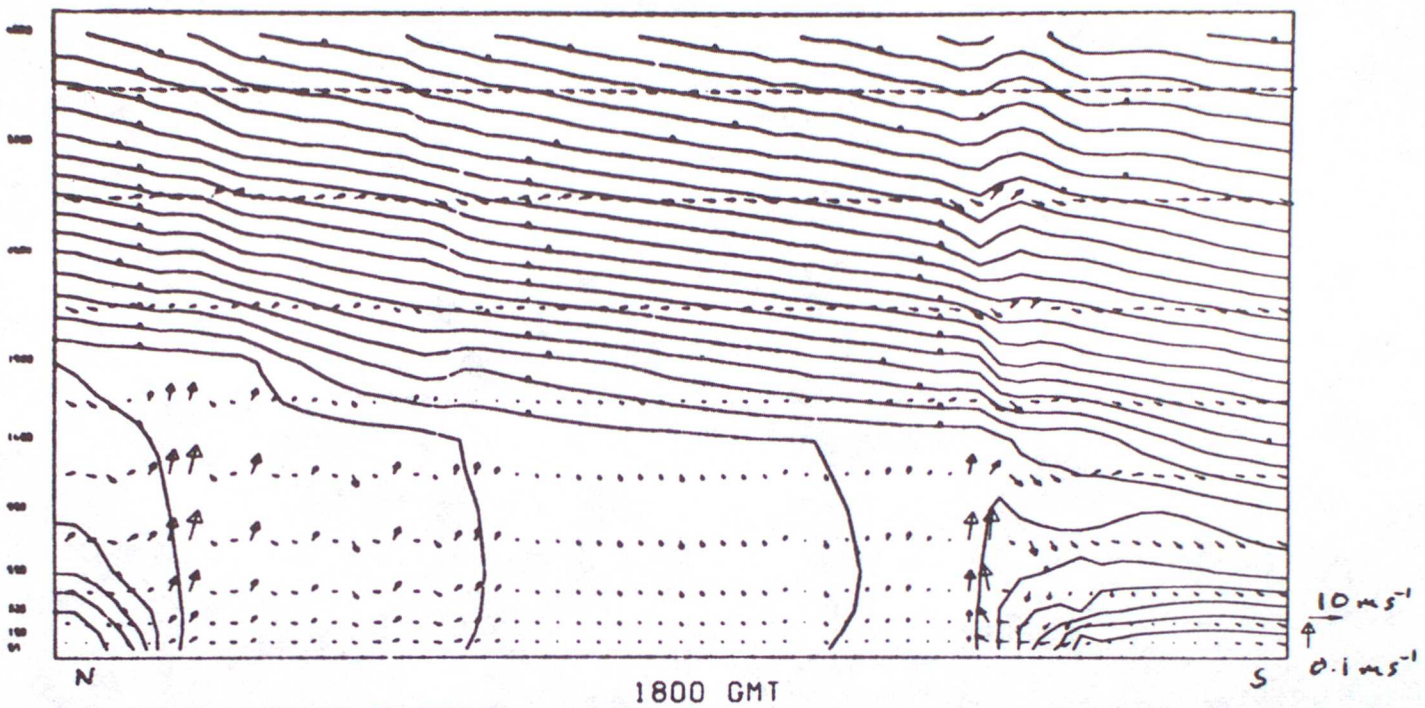

1800 GMT

WIND VECTORS & POTENTIAL TEMPERATURE

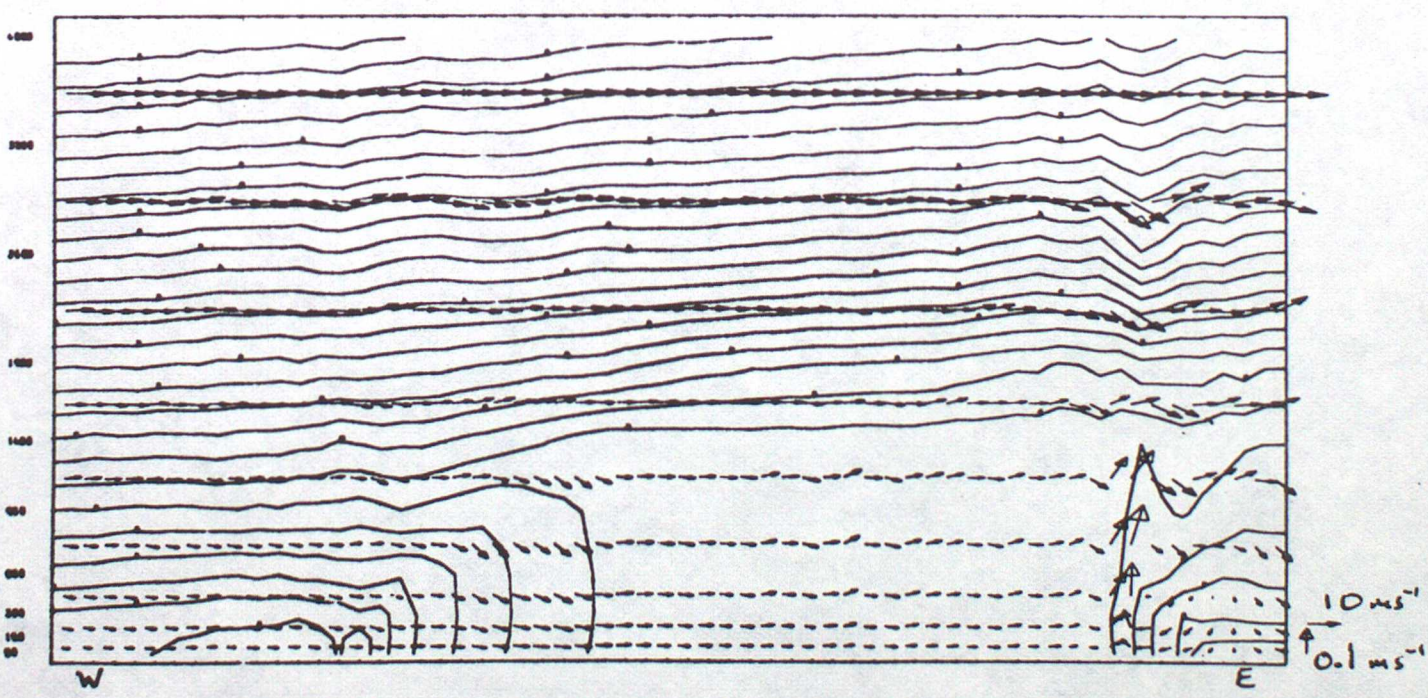

FIG. 10

14 HR F'CAST MSL PRESSURE & LOW LEVEL WINDS

1800 GMT

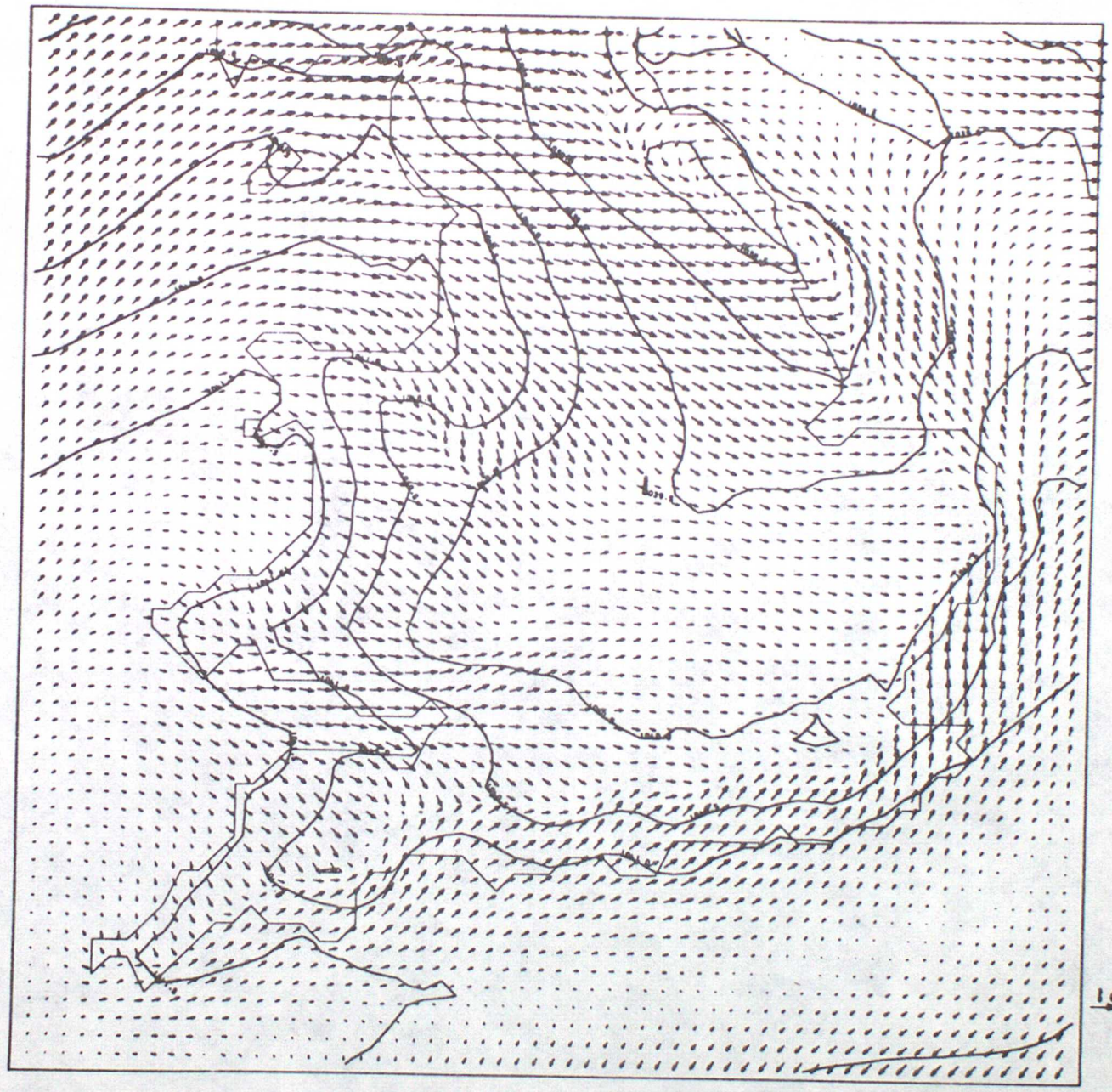

FIG. 11

TOPOGRAPHIC HEIGHT (CONTOUR INTERVAL 50 METRES)

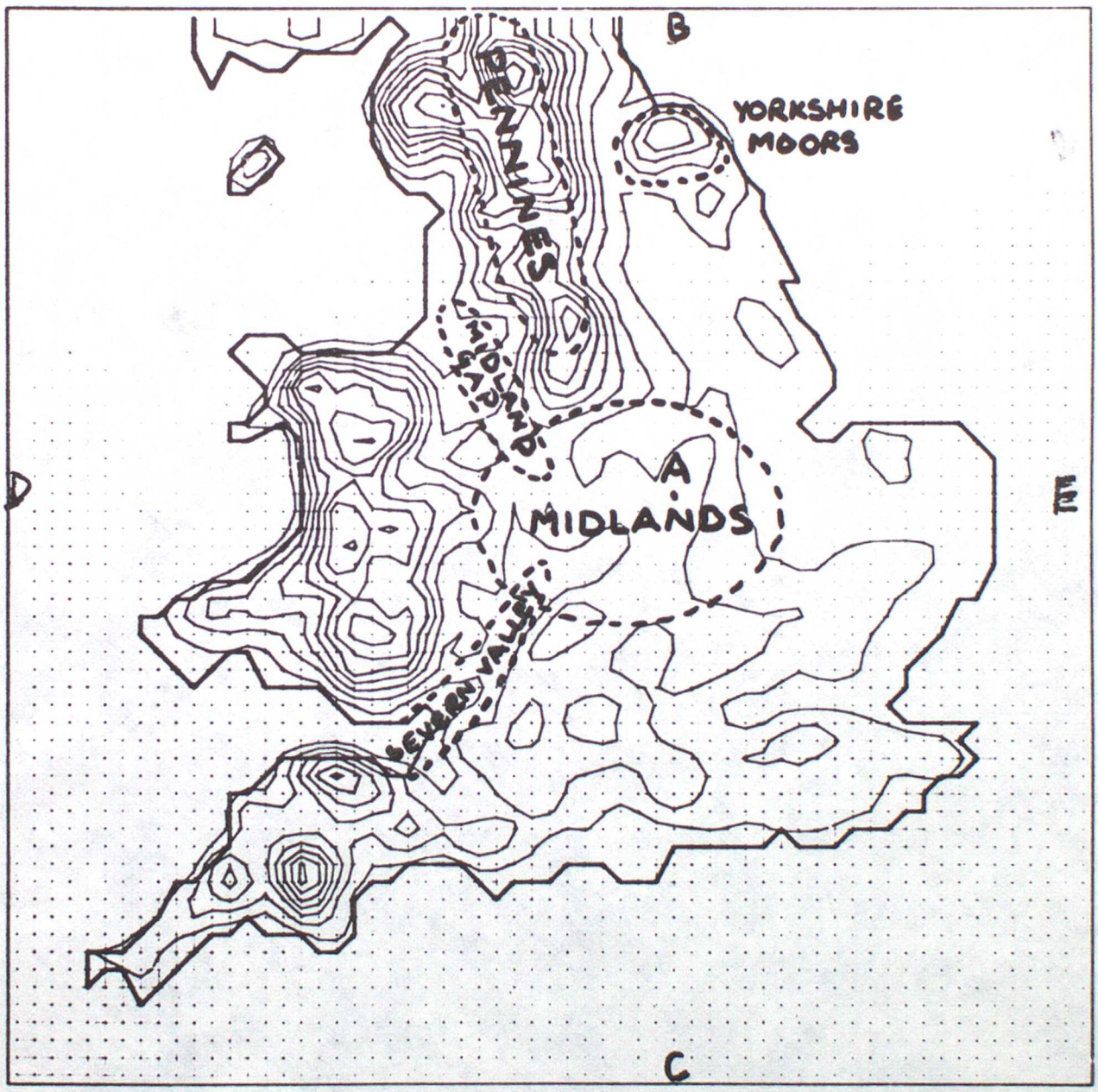

FIG. 12

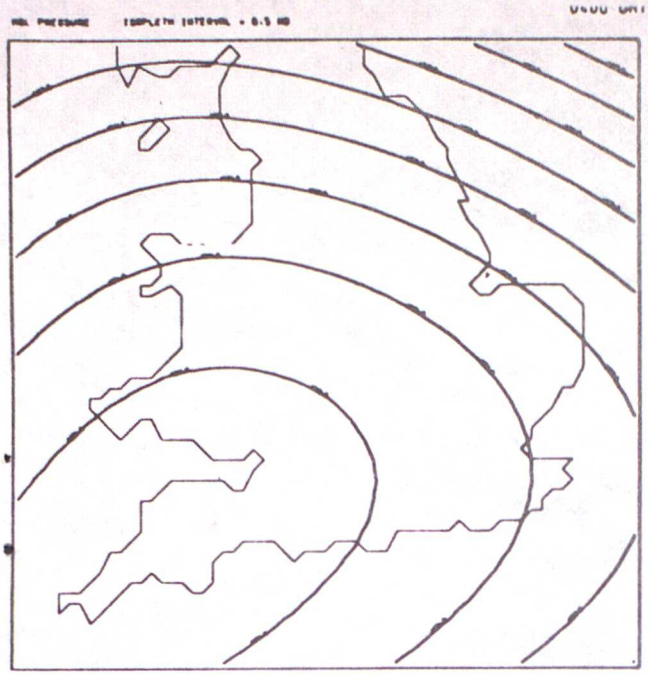

FIG 13(a)

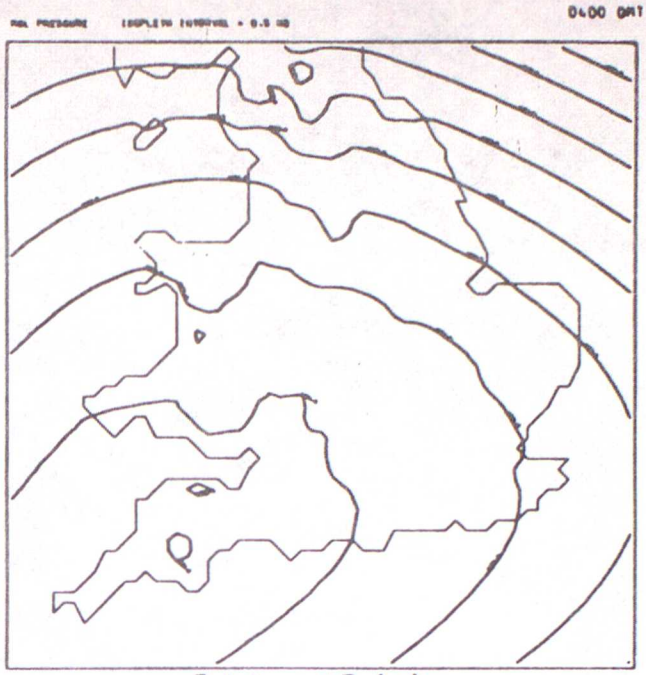

FIG 13(b)

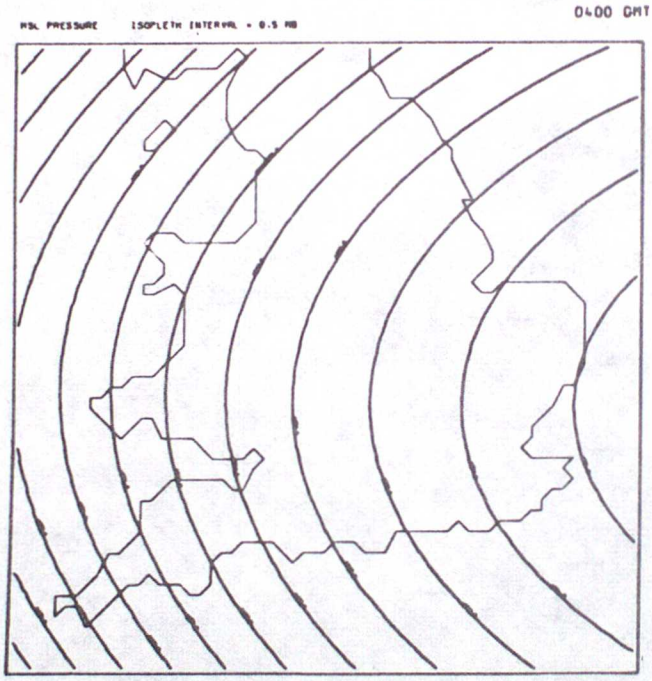

FIG 14(a)

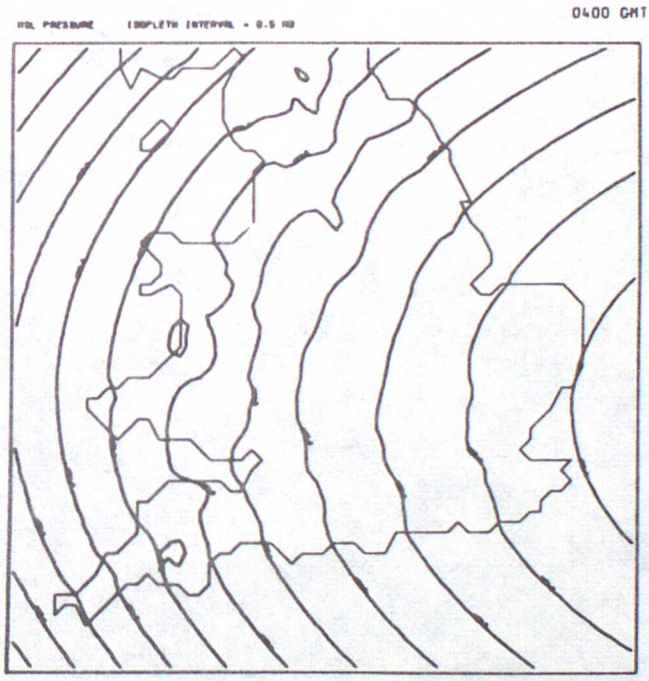

FIG 14(b)

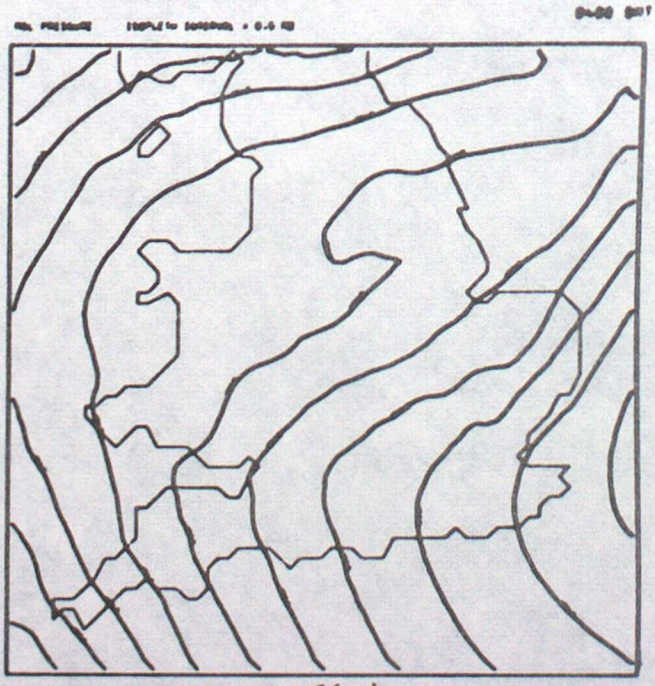

FIG 15(a)

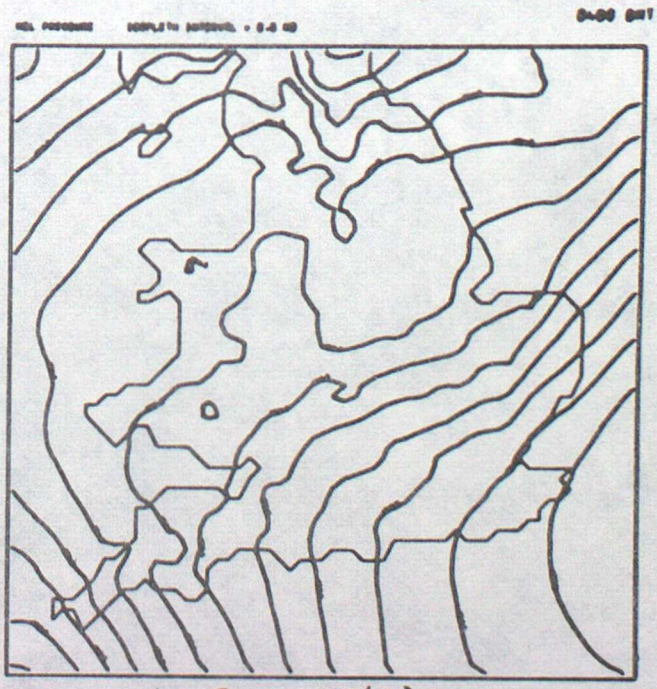

FIG 15(b)

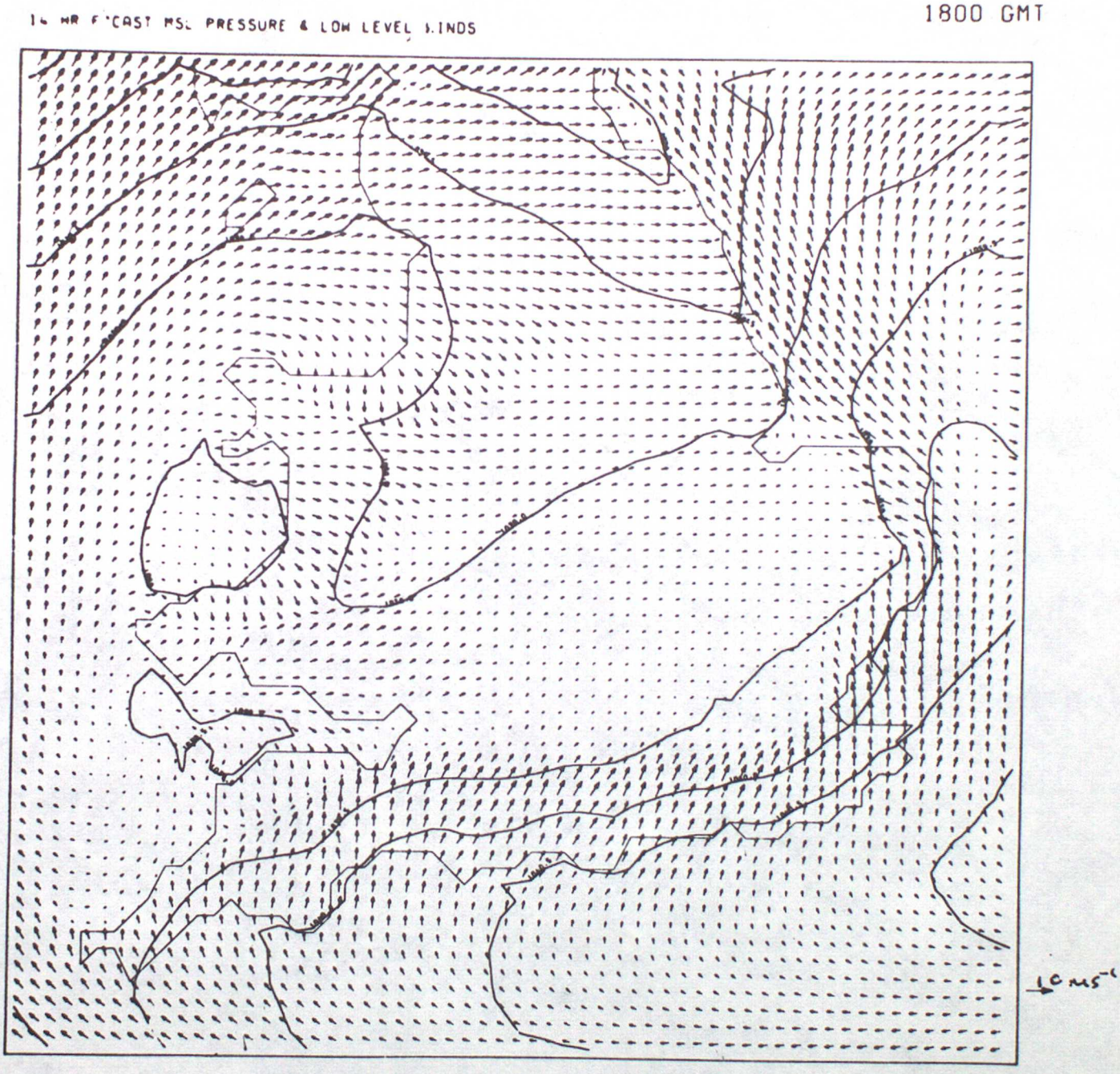

FIG. 16

24 HR F'CAST MSL PRESSURE & LOW LEVEL WINDS

1800 GMT

FIG. 17.

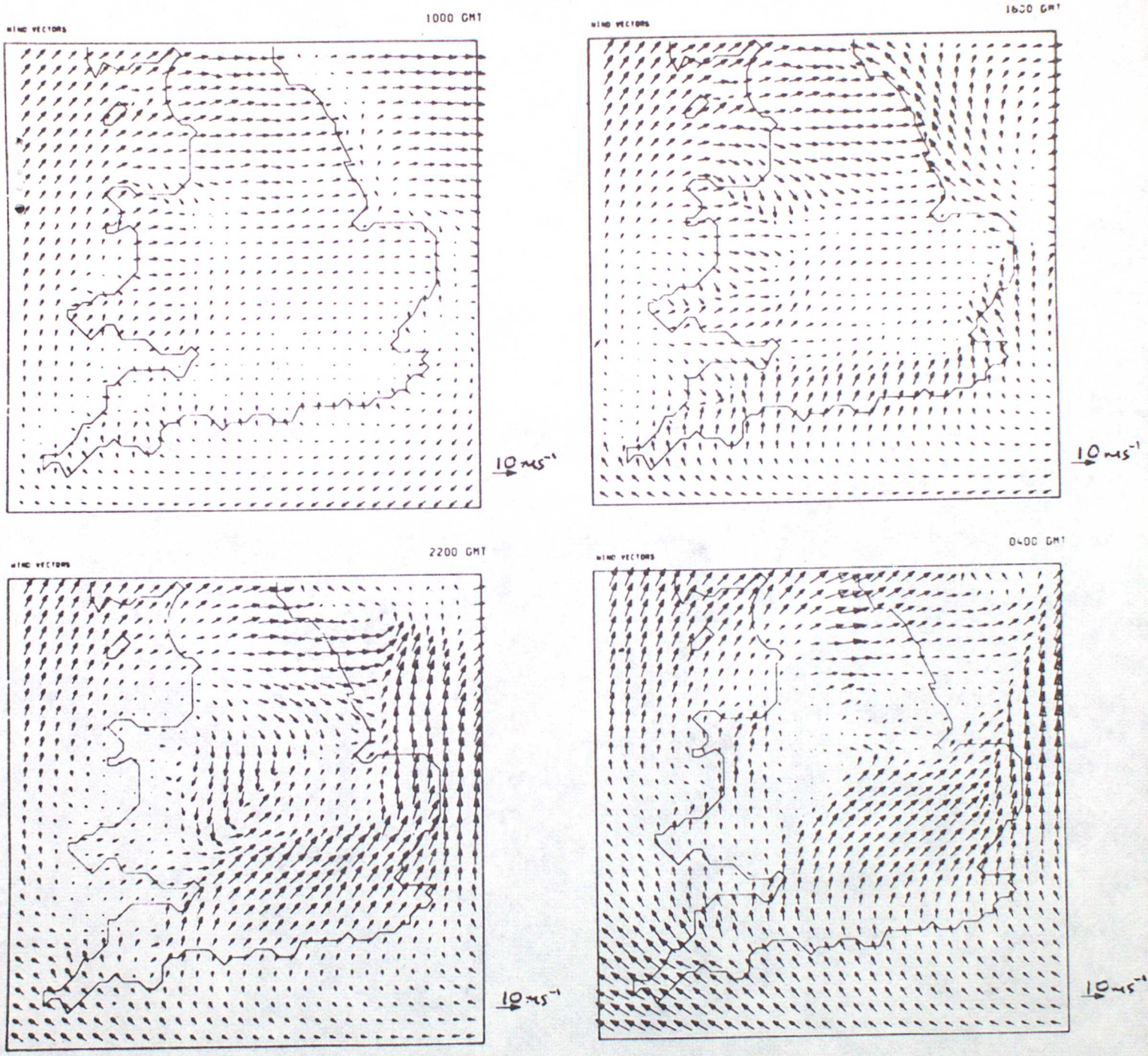
1000 GMT
WIND VECTORS
10 ms⁻¹
1630 GMT
WIND VECTORS
10 ms⁻¹
2200 GMT
WIND VECTORS
10 ms⁻¹
0400 GMT
WIND VECTORS
10 ms⁻¹

FIG. 18

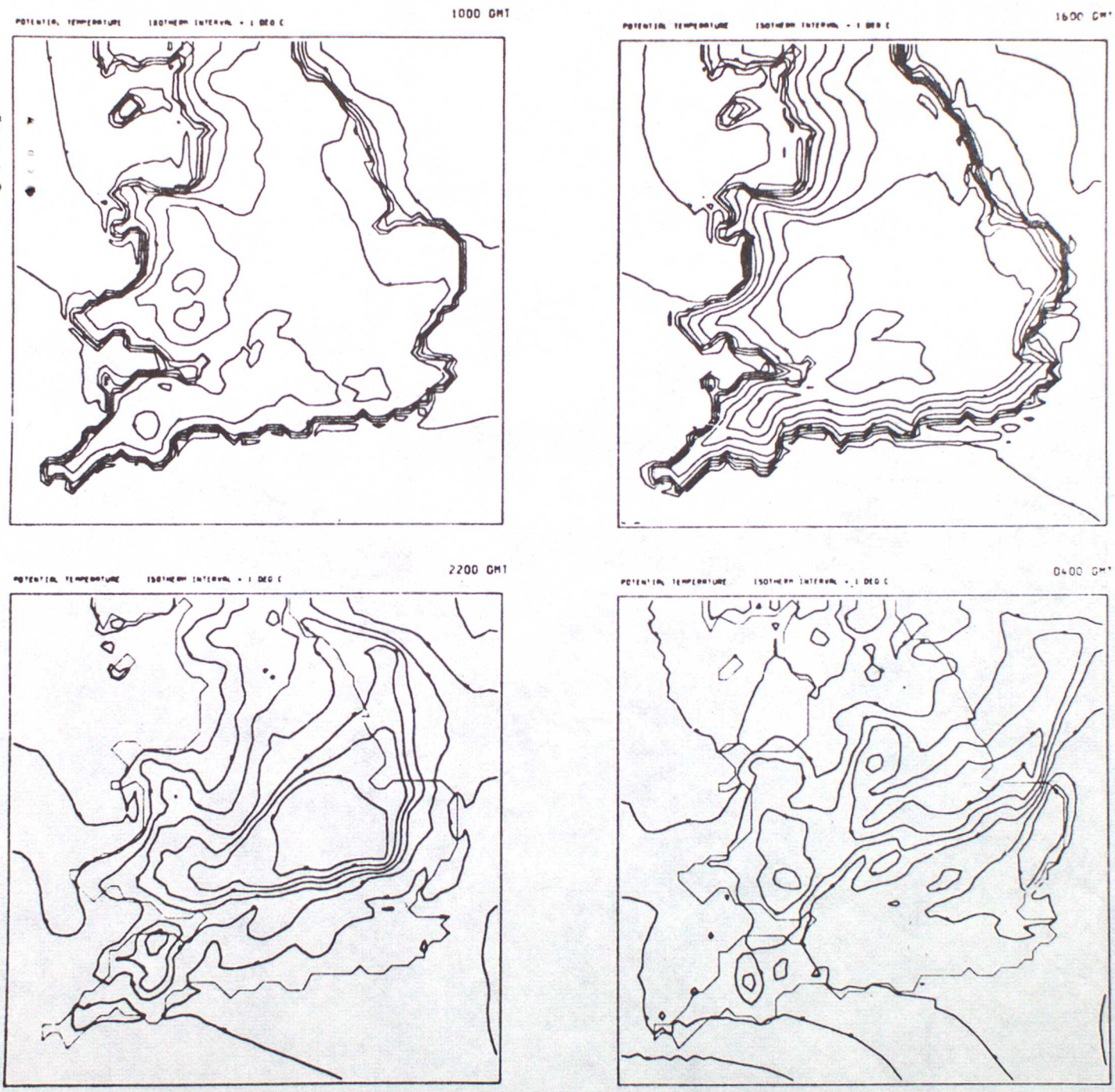
POTENTIAL TEMPERATURE ISOTHERM INTERVAL = 1 DEG C
1000 GMT
POTENTIAL TEMPERATURE ISOTHERM INTERVAL = 1 DEG C
1600 GMT
POTENTIAL TEMPERATURE ISOTHERM INTERVAL = 1 DEG C
2200 GMT
POTENTIAL TEMPERATURE ISOTHERM INTERVAL = 1 DEG C
0400 GMT

FIG. 19

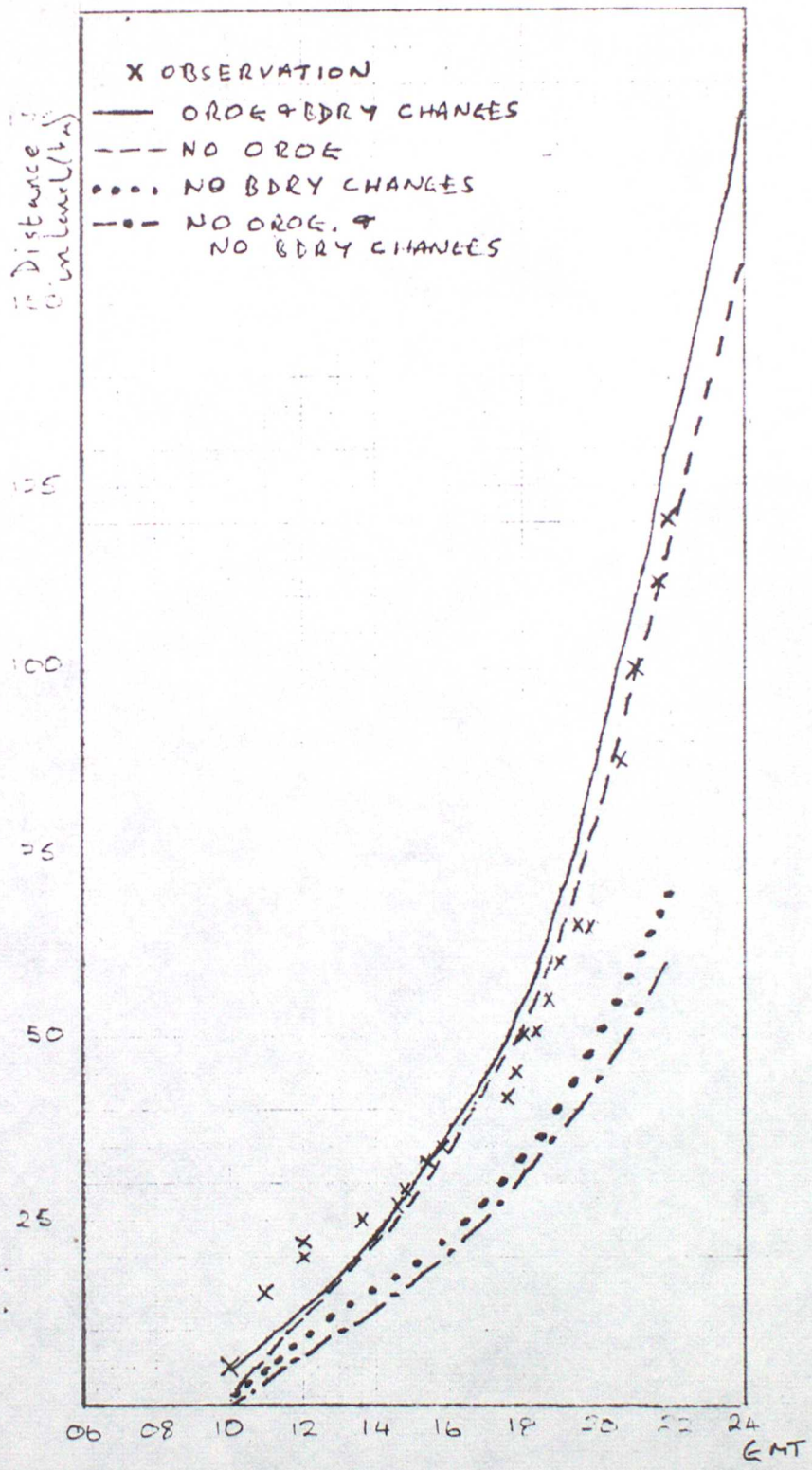
X OBSERVATION
OROG & BDRY CHANGES
NO OROG
NO BDRY CHANGES
NO OROG. & NO BDRY CHANGES
Distance in Level (km)
150
125
100
75
50
25
06
08
10
12
14
16
18
20
22
24
GMT

FIG. 20

2200 GMT

NORMAL VELOCITY ISOPLETH INTERVAL = 2 M/SEC

2200 GMT

WIND VECTORS & POTENTIAL TEMPERATURE

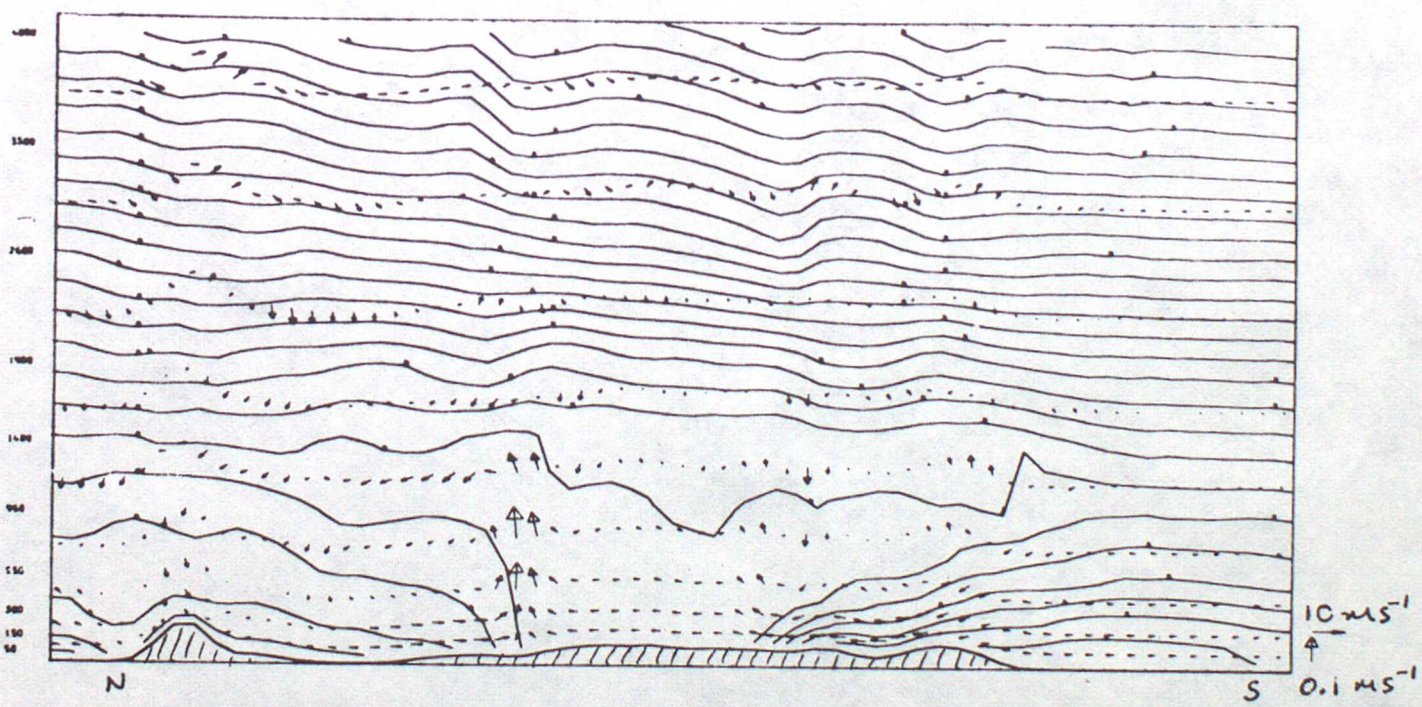

FIG. 21

TRAJECTORY

INITIAL DATA TIME = 12 14/6/73

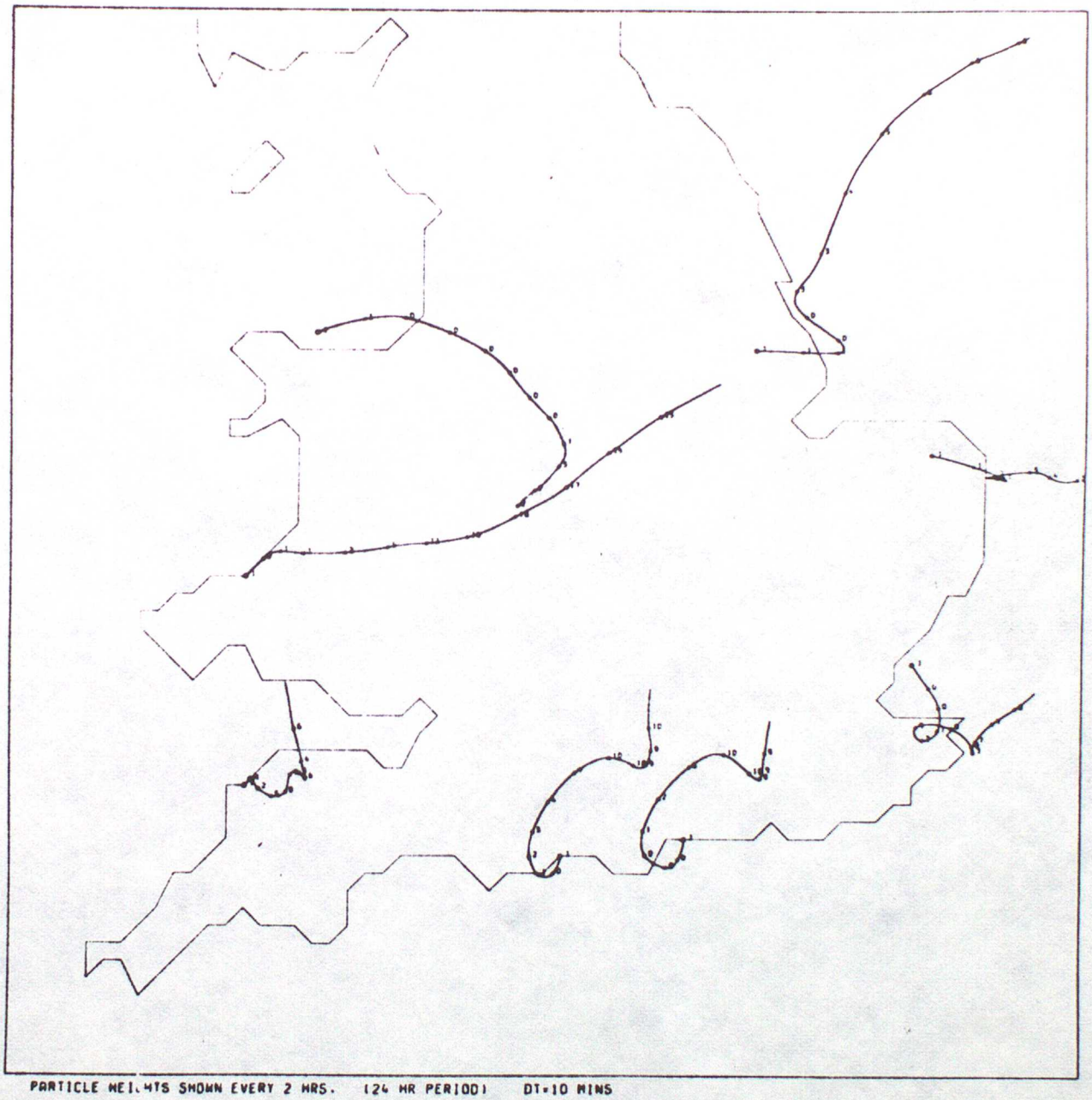

PARTICLE HEIGHTS SHOWN EVERY 2 HRS. (24 HR PERIOD) DT=10 MINS

FIG. 22